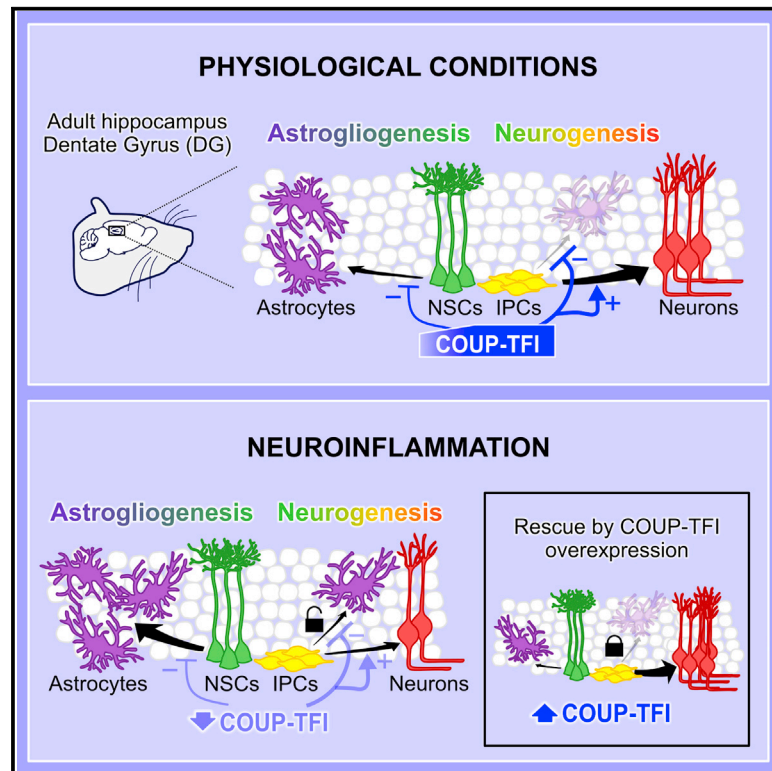# Neuron-Astroglia Cell Fate Decision in the Adult Mouse Hippocampal Neurogenic Niche Is Cell-Intrinsically Controlled by COUP-TFI *In Vivo*

Graphical Abstract

Highlights

- COUP-TFI is expressed by adult NSCs/progenitors in the hippocampal dentate gyrus (DG)

- COUP-TFI promotes neurogenic fate by repressing astrogliogenesis in the adult DG

- Neuroinflammation downregulates COUP-TFI expression in adult hippocampal NSCs

- Increased COUP-TFI levels rescue neuro-gliogenesis imbalance in the inflamed DG

Authors

Sara Bonzano, Isabella Crisci,
Anna Podlesny-Drabiniok,
Chiara Rolando, Wojciech Krezel,
Michèle Studer, Silvia De Marchis

Correspondence

michele.studer@unice.fr (M.S.),
silvia.demarchis@unito.it (S.D.M.)

In Brief

The adult hippocampal dentate gyrus contains multipotent neural stem cells (NSCs) and neuronal committed progenitors. Bonzano et al. demonstrate that the nuclear receptor COUP-TFI cell-intrinsically drives NSCs/progenitors toward neurogenesis by repressing astrogliogenesis. Notably, COUP-TFI downregulation occurs in inflamed hippocampi, and its overexpression rescues the hippocampal neurogenesis-astrogliogenesis imbalance due to neuroinflammation.

CellPress

Neuron-Astroglia Cell Fate Decision in the Adult Mouse Hippocampal Neurogenic Niche Is Cell-Intrinsically Controlled by COUP-TFI *In Vivo*

Sara Bonzano,[1,2,3] Isabella Crisci,[1,2] Anna Podlesny-Drabiniok,[4,5,6,7] Chiara Rolando,[8] Wojciech Krezel,[4,5,6,7] Michèle Studer,[3,9,*] and Silvia De Marchis[1,2,9,10,*]
[1]Neuroscience Institute Cavalieri Ottolenghi (NICO), University of Turin, Orbassano 10043, Italy
[2]Department of Life Sciences and Systems Biology, University of Turin, Turin 10123, Italy
[3]Université Côte d'Azur (UCA) CNRS, Inserm, iBV, Nice 06108, France
[4]Institut de Génétique et de Biologie Moléculaire et Cellulaire, Illkirch 67404, France
[5]Inserm, U1258, Illkirch, France
[6]CNRS, UMR 7104, Illkirch, France
[7]Université de Strasbourg, Illkirch, France
[8]Department of Biomedicine, University of Basel, Basel 4031, Switzerland
[9]Senior author
[10]Lead Contact
*Correspondence: michele.studer@unice.fr (M.S.), silvia.demarchis@unito.it (S.D.M.)
 https://doi.org/10.1016/j.celrep.2018.06.044

SUMMARY

In the dentate gyrus (DG) of the mouse hippocampus, neurogenesis and astrogliogenesis persist throughout life. Adult-born neurons and astrocytes originate from multipotent neural stem cells (NSCs) whose activity is tightly regulated within the neurogenic niche. However, the cell-intrinsic mechanisms controlling neuron-glia NSC fate choice are largely unknown. Here, we show COUP-TFI/NR2F1 expression in DG NSCs and its downregulation upon neuroinflammation. By using *in vivo* inducible knockout lines, a retroviral-based loss-of-function approach and genetic fate mapping, we demonstrate that *COUP-TFI* inactivation in adult NSCs and/or mitotic progenitors reduces neurogenesis and increases astrocyte production without depleting the NSC pool. Moreover, forced COUP-TFI expression in adult NSCs/progenitors decreases DG astrogliogenesis and rescues the neuro-astrogliogenic imbalance under neuroinflammation. Thus, COUP-TFI is necessary and sufficient to promote neurogenesis by suppressing astrogliogenesis. Our data propose COUP-TFI as a central regulator of the neuron-astroglia cell fate decision and a key modulator during neuroinflammation in the adult hippocampus.

INTRODUCTION

Once considered limited to the embryonic and perinatal periods, neural stem cells (NSCs) persist in two discrete regions of the adult mammalian brain: the subventricular zone (SVZ) lining the lateral ventricles and the subgranular zone (SGZ) of the hippo-

campal dentate gyrus (DG) (Kempermann et al., 2015). Within the adult SGZ, NSCs are mostly quiescent, show a typical radial morphology, and are referred to as radial glia-like (RGL) or type 1 stem cells. Upon activation, a RGL cell can divide symmetrically to produce two RGL cells or asymmetrically to self-renew and generate a differentiated progeny. In the latter case, RGL cells can give rise to rapidly dividing intermediate progenitors (type 2; IPCs), which generate neuroblasts and eventually exit the cell cycle to differentiate into mature granule cells (GCs) (Bond et al., 2015; Kempermann et al., 2015). Adult DG neurogenesis plays a crucial role in learning and memory, and it is regulated by several factors, including stress, inflammation, environmental enrichment, and voluntary physical activity (Kempermann, 2015).

Alongside neurogenesis, astrogliogenesis allows a continuous production of astrocytes in the adult DG, either by RGL asymmetric division (i.e., maintaining the RGL cell pool) or by direct differentiation implying a depletion in the RGL cell pool (Bona-guidi et al., 2011; Encinas et al., 2011). Astrocytes are key constituents of the neurogenic niche and play fundamental roles in the regulation of NSCs/progenitors by promoting neurogenesis (Barkho et al., 2006; Song et al., 2002). Interestingly, running enhances DG neurogenesis, as well as astrogliogenesis (Steiner et al., 2004), whereas pathological conditions, such as inflammation, lead to NSC dysfunction, altering the neuron-astrocyte production rate in favor of astrocytes (Woodbury et al., 2015; Wu et al., 2012). This highlights the importance of a tight control of neuronal versus astroglial cell fate decision, most probably linked to intrinsic regulation in the NSC/progenitor pool. However, the nature of a transcriptional program underlying this function is still unknown.

COUP-TFI (also called NR2F1) is a nuclear hormone receptor acting as a strong transcriptional regulator whose functions range from the control of embryonic NSC behavior (Naka-Ka-neda et al., 2014; Naka et al., 2008) to the regulation of cell migration in the neocortex and developing DG (Alfano et al., 2011; Ber-tacchi et al., 2018; Parisot et al., 2017). Cortical depletion of COUP-TFI during early stages results in abnormal motor skill
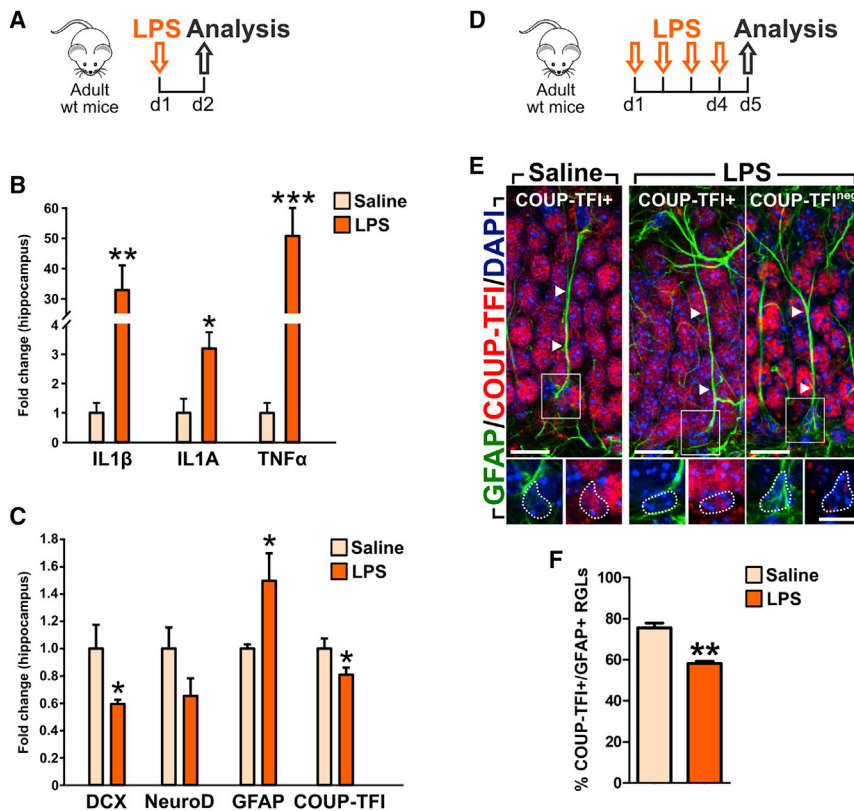
Figure 1. Acute Neuroinflammation Leads to COUP-TFI Downregulation within the Adult DG

(A) Experimental design for transcript expression analysis on hippocampal tissue extracts.

(B and C) Changes in pro-inflammatory cytokines (B), neuronal (DCX, NeuroD), glial (GFAP), and COUP-TFI gene transcripts (C) in the hippocampi of LPS-treated mice revealed by RT-qPCR (n = 5 mice/treatment; technical replicates = 2).

(D) Experimental design for immunofluorescence analysis on the DG.

(E) Confocal images of GFAP+ (green) RGLs either positive (+) of negative (neg) for COUP-TFI (red) in DG sections of saline- and LPS-treated mice. Cell nuclei are counterstained with DAPI (blue). Arrowheads indicate radial cell processes. Scale bar, 10 μm.

(F) Quantification of COUP-TFI+ nuclei among GFAP+ RGL cells (RGLs) in saline (n = 257 of 353 double+ cells out of three mice) and LPS-treated mice (n = 220 of 379 double+ cells out of three mice).

Error bars indicate SEM. Student's t test: *p < 0.05, **p < 0.01, and ***p < 0.001. See also Figure S1.

behavior and spatial memory deficits (Flore et al., 2016; Tomassy et al., 2010), and haploinsufficiency of COUP-TFI in patients leads to global developmental delay, intellectual disabilities, and optic atrophy (Al-Kateb et al., 2013; Bosch et al., 2014; Bertacchi et al., 2018). COUP-TFI continues to be expressed in the adult CNS, including neurogenic niches (Bovetti et al., 2013; Llorens-Bobadilla et al., 2015), but its functional role in adult NSCs is unknown.

Here, we examined the expression and function of COUP-TFI in the adult DG neurogenic niche. First, we showed that COUP-TFI levels were downregulated upon induced neuroinflammation followed by increased astrogliogenesis. Next, to assess whether COUP-TFI was directly involved in this process, we genetically manipulated *COUP-TFI* by targeting adult NSCs and/or mitotic progenitors through loss- and gain-of-function experiments *in vivo*. By using two independent conditional inducible mouse transgenic lines and a retroviral-based approach, coupled to genetic fate mapping, we found that *COUP-TFI* deletion in NSCs and/or committed neurogenic progenitors decreased hippocampal neurogenesis and increased astrogliogenesis, indicating a switch of NSCs/progenitors toward a gliogenic commitment. Finally, complementary gain-of-function experiments showed that COUP-TFI overexpression in adult DG NSCs/progenitors was sufficient to repress astrogliogenesis and, importantly, to rescue neurogenesis during inflammation. Overall, these data unravel a key role for COUP-TFI as a transcriptional regulator in the decision-making process of generating either new neurons or astrocytes within the healthy and inflamed adult hippocampus.

RESULTS

Acute Neuroinflammation Leads to COUP-TFI Downregulation within the Adult DG

Neuroinflammation severely affects adult neurogenesis and increases astrocyte production in the adult hippocampal DG (Kohman and Rhodes, 2013; Monje et al., 2003; Wu et al., 2012). However, little is known about the mechanisms underlying this process within the DG NSC/progenitor pool. With the goal of identifying novel cell-intrinsic regulators responding to neuroinflammation and involved in controlling neurogenesis and/or astrogliogenesis within the adult hippocampus, we acutely administrated the *E. coli*-derived lipopolysaccharide (LPS) by intraperitoneal (i.p.) injection to initiate an inflammatory response (Figure 1A). The occurrence of an inflammatory response was confirmed by a strong transcript increase of the pro-inflammatory cytokines interleukin-1β (IL-1β), interleukin-1A (IL-1A), and tumor necrosis factor α (TNFα) in the hippocampi of LPS-treated mice compared with control saline-injected mice at 1 day post-injection (Figure 1B). In parallel, LPS treatment downregulated the expression of the immature neuronal markers doublecortin (DCX) and NeuroD and upregulated the glial fibrillary acid protein (GFAP) (Figure 1C), in line with an alteration in the newborn neuron/astrocyte ratio, as previously reported during neuroinflammation (Wu et al., 2012). Interestingly, we also found that the nuclear receptor COUP-TFI was downregulated in LPS-treated mice (Figure 1C), indicating a direct response of this transcriptional regulator to inflammation in the adult hippocampus.
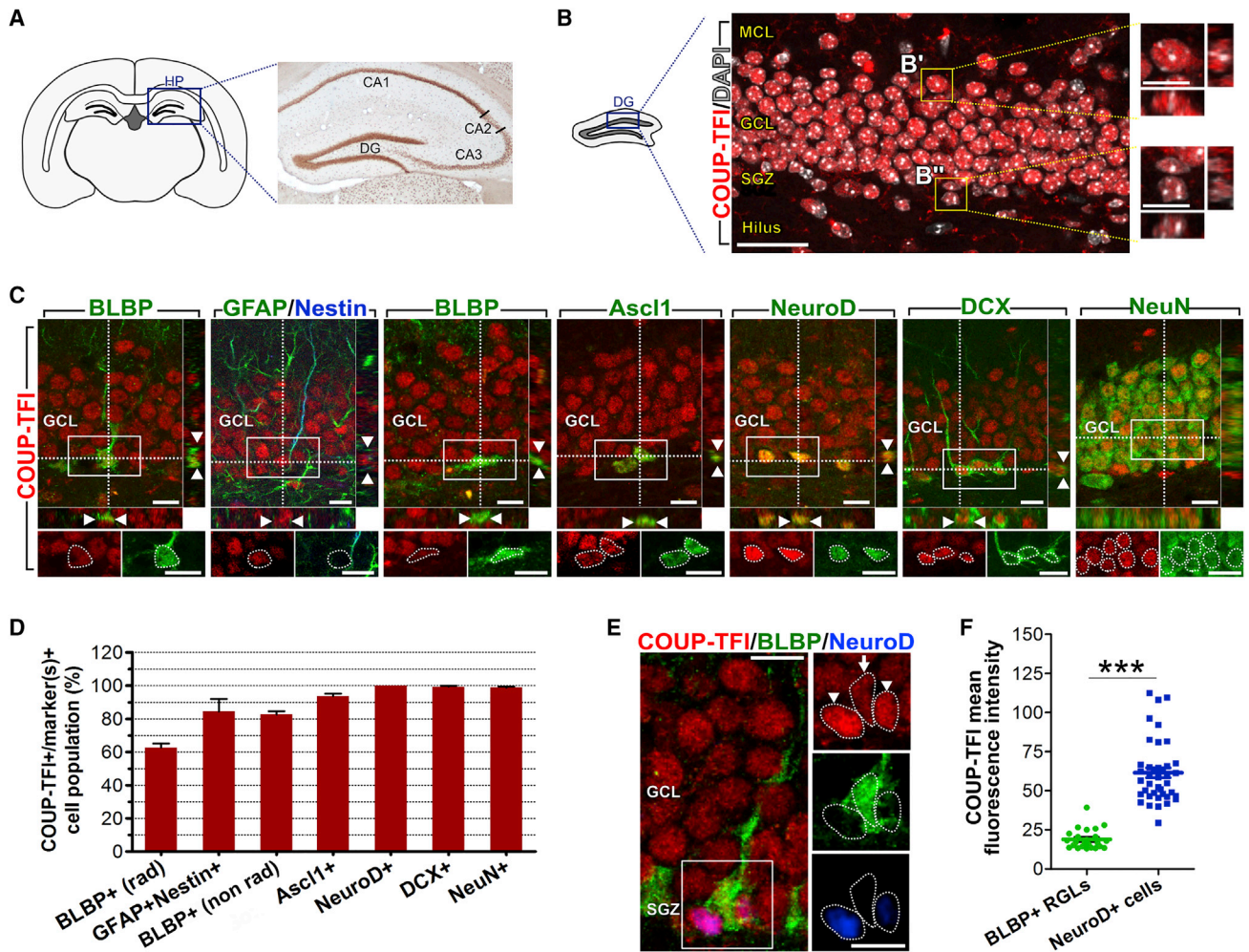
Figure 2. COUP-TFI Is Expressed in NSCs and in the Neurogenic Lineage of the Adult DG

(A) Schematic drawing of a coronal section of an adult mouse brain. The box indicates the hippocampus (HP), where COUP-TFI immunostaining is shown.

(B) Confocal images of COUP-TFI+ cells (red) in an adult DG section counterstained with DAPI (white).

(C) Confocal images of the DG immunostained for COUP-TFI (red) and different cell type-specific markers of the adult hippocampal neurogenic lineage (green, blue). Double-labeled cells are shown at higher magnifications (bottom) as single color channel images.

(D) Quantification of COUP-TFI+ cells among the pools of DG cells expressing different markers listed on the x axis (>200 cells/marker).

(E) Confocal images illustrating differences in COUP-TFI levels in radial BLBP+ stem cells (arrow) versus NeuroD+ neuronal-committed cells (arrowheads).

(F) Dot plot reporting the intensity of COUP-TFI immunolabeling in BLBP+ RGL cells (n = 24 double+ cells) and NeuroD+ neuronal progenitors (n = 40 double+ cells).

N = 3 adult mice. GCL, granule cell layer; MCL, molecular cell layer; SGZ, subgranular zone. Error bars indicate SEM. Scale bars, 50 μm (B) and 10 μm (insets in B; C and E). Student's t test: ***p < 0.001. See also Figure S2.

To identify changes in COUP-TFI at the cellular level, we treated adult mice once a day for 4 consecutive days with LPS (d1–d4) and analyzed COUP-TFI protein expression in the hippocampal RGL cell pool at day 5 (Figures 1D and 1E). In accordance with transcript downregulation (Figure 1C), we found a decrease of GFAP+ RGL cells expressing COUP-TFI in LPS-treated DG (Figures 1E and 1F). As expected, we also found a reduced number of DCX+ immature newborn neurons and an expansion of GFAP+ astrocytes within the GCL of LPS-treated mice (Figures S1A–S1D). Thus, on the basis of COUP-TFI downregulation in RGL cells upon inflammatory insult, we hypothe-

sized that COUP-TFI could be directly involved in the imbalance in neuron to astrocyte generation within the DG.

COUP-TFI Is Expressed in NSCs and in the Neurogenic Lineage of the Adult DG

To understand whether COUP-TFI could act as a potential regulator of neuron versus astroglia RGL cell commitment, we first investigated its cell type-specific distribution in the DG of the adult hippocampus (Figure 2). COUP-TFI protein expression was analyzed in the granule cell layer (GCL) and neurogenic SGZ along the entire DG anteroposterior axis by using a series
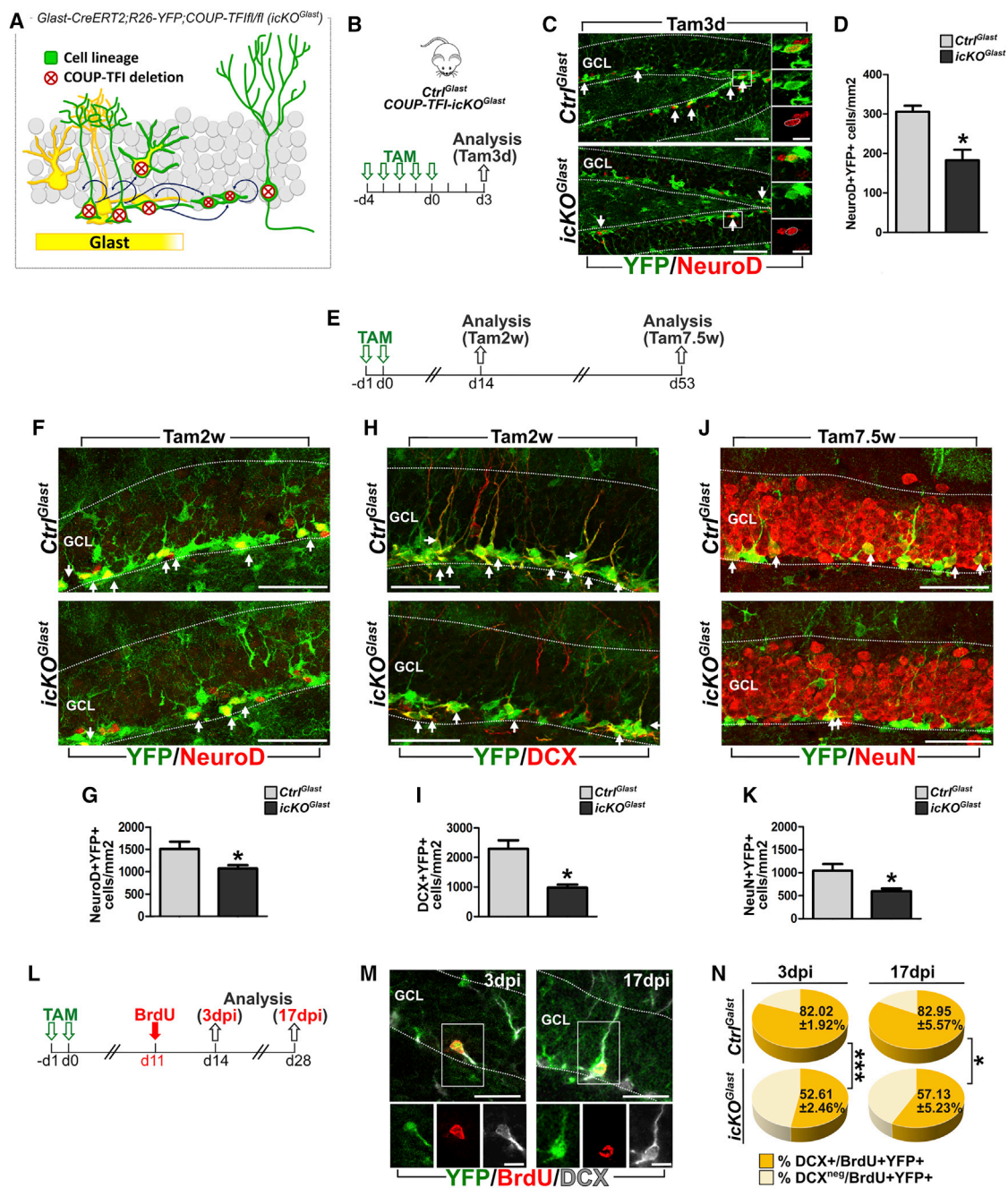
Figure 3. COUP-TFI Depletion in Adult RGL Cells Impairs DG Neurogenesis

(A) Schema illustrating *COUP-TFI* deletion (red crossed circles) in the cell progeny (green) derived from *Glast*-expressing cells (yellow) in the DG upon tamoxifen (TAM) induction in *COUP-TFI-icKO*^Glast^ adult mice.

(B) Experimental design to assess the early consequences of COUP-TFI loss-of-function in the Glast-lineage (see C and D).

(C) Confocal images of double immunostaining for YFP (green) and NeuroD (red) in *Ctrl*^Glast^ and *COUP-TFI-icKO*^Glast^ DG.

(D) Quantification of double NeuroD+YFP+ cells in *Ctrl*^Glast^ and *COUP-TFI-icKO*^Glast^ DG.

(E) Experimental design for long-term effects of COUP-TFI loss-of-function in the Glast-lineage (see F–K).

(F, H, and J) Confocal images of NeuroD+ (F, red), DCX+ (H, red), and NeuN+ (J, red) double-positive for YFP (green) in *Ctrl*^Glast^ and *COUP-TFI-icKO*^Glast^ DG at Tam2w (F and H) and Tam7.5w (J).

(G, I, and K) Quantification of double NeuroD+YFP+ (G), DCX+YFP+ (I), and NeuN+YFP+ (K) cells in *Ctrl*^Glast^ and *COUP-TFI-icKO*^Glast^ DG.

(L) Experimental design used to label a cohort of newborn cells with BrdU in TAM-treated mice in the Glast-lineage (see M and N).

(M) Confocal images of newborn neurons triple-positive for BrdU (red), YFP (green), and DCX (gray) at 3 and 17 days post BrdU injection (dpi) in *Ctrl*^Glast^ DG.

(legend continued on next page)

of cell stage-specific markers combined with morphological analysis (Figures 2A–2D and S2). In the SGZ, more than 60% of all RGL cells, identified by their radial morphology and BLBP expression (Steiner et al., 2004), and the large majority of double GFAP+Nestin+ RGL cells (DeCarolis et al., 2013) co-expressed COUP-TFI (Figures 2C and 2D). Non-radial BLBP+ cells, accounting for horizontal type 1 and neuronal committed type 2a progenitors, and Ascl1+ cells, including activated stem cells and type 2a progenitors (Andersen et al., 2014; Lugert et al., 2010, 2012), also largely expressed COUP-TFI (Figures 2C and 2D). Thus, in the adult SGZ, COUP-TFI is localized in active NSCs and neurogenic progenitors, as further supported by co-expression with the proliferative marker Ki67+ (Figure S2B). Finally, the use of neuron-specific markers revealed that virtually all late neuronal progenitors (type 2b), neuroblasts, and immature neurons, labeled by NeuroD or DCX (Gao et al., 2009; Steiner et al., 2006), as well as NeuN+ mature neurons (Ming and Song, 2005), were also COUP-TFI+ (Figures 2C and 2D). However, the intensity of COUP-TFI immunofluorescence was doubled in NeuroD+ cells compared with BLBP+ RGL cells (Figures 2E and 2F), suggesting an upregulation of COUP-TFI expression in neuronal committed cells. Overall, these data reveal that COUP-TFI is widely expressed in the SGZ/GCL throughout the neurogenic lineage, although at different levels, implying tight regulation for this transcription factor in different cellular components of the adult DG niche.

COUP-TFI Depletion in Adult RGL Cells Impairs DG Neurogenesis

To directly investigate COUP-TFI function in the adult hippocampal neurogenic niche, we adopted a genetic loss-of-function approach coupled to fate mapping in adult RGL cells. The *COUP-TFIfl/fl* mouse line (Armentano et al., 2007) was crossed with mice carrying the tamoxifen (TAM)-inducible form of *Cre-recombinase* (*CreERT2*) under *Glast* transcriptional control (Mori et al., 2006) and to a *Rosa26-YFP* reporter line (Srinivas et al., 2001) (Figure S3A). The resulting progeny was named *COUP-TFI-icKO^Glast* and allowed fate mapping of RGL cells that had undergone selective *COUP-TFI* deletion (Figure 3A). *Glast-CreERT2* mice carrying the *R26-YFP* reporter transgene, but wild-type for *COUP-TFI*, were used as controls (*Ctrl^Glast*).

First, we assessed the early effects of COUP-TFI loss in the adult RGL cells by treating *COUP-TFI-icKO^Glast* and *Ctrl^Glast* mice for 5 consecutive days with TAM and analyzing the DG 3 days after (Figure 3B). Notably, the drastic drop in COUP-TFI expression in mutants (Figures S3B and S3C) was associated with a decrease in double NeuroD+YFP+ neuronal committed progenitors and neuroblasts (Figures 3C and 3D). However, COUP-TFI loss did not affect the densities of either the total recombined YFP+ population or double GFAP+YFP+ RGL cells within the DG of mutant mice compared with controls (Figures S3D–S3F). Moreover, mice injected i.p. with BrdU the day before

analysis (Figure S3G) showed no significant differences in the density of double BrdU+YFP+ cells in *COUP-TFI-icKO^Glast* DG *versus Ctrl^Glast* (Figures S3H and S3I), indicating no alteration in NSC/progenitor proliferation. Thus, these data suggest that COUP-TFI normally promotes neurogenesis within adult hippocampal NSCs without affecting their proliferation rate.

Next, we shortened TAM treatment to 2 days, to achieve mosaic recombination of RGL cells within a wild-type environment and to assess the effect of *COUP-TFI* deletion at longer survival time (Figure 3E). The large majority of recombined YFP+ cells failed to express COUP-TFI after 2 weeks (d14) and 7.5 weeks (d53) (Figure S3J), confirming *COUP-TFI* Cre-induced deletion. The recombined YFP+ population expressing NeuroD or DCX was significantly reduced in *COUP-TFI-icKO^Glast* mice compared with controls at d14 (Figures 3F–3I), similar to the density of double NeuN+YFP+ mature neurons quantified at d53 (Figures 3J and 3K). Accordingly, the percentage of NeuroD+, DCX+, and NeuN+ cells among the YFP+ population significantly dropped in mutant DG (Table S1), supporting diminished neurogenesis upon COUP-TFI inactivation in the adult hippocampal RGL cell lineage.

To further address a possible defect in newborn neuron survival upon COUP-TFI deletion, mutant and control mice were treated for 2 days with TAM and injected 11 days later with BrdU (Figure 3L). DG were analyzed 3 days post-BrdU injection (dpi), during the peak of newborn BrdU+ cells (Steiner et al., 2004), and 17 dpi, after the early selection phase and when surviving newborn cells reach stable levels (Encinas et al., 2011) (Figure 3L). No significant differences were found in the density of double BrdU+YFP+ cells at both time points (Figures S3K and S3L). Moreover, double BrdU+YFP+ cells at 17 dpi corresponded to nearly 25% of that found at 3 dpi in both *Ctrl^Glast* and *COUP-TFI-icKO^Glast* (Figure S3M), indicating no alteration in newborn cell survival during this critical period. However, the number of DCX+ cells among the double BrdU+YFP+ population significantly decreased in *COUP-TFI-icKO^Glast* compared with *Ctrl^Glast* at both survival times (Figures 3M and 3N). This effect was specific to mutated YFP+ cells, as BrdU+ YFP negative cells (i.e., not recombined) showed no differences in the percentage of DCX+ cells in *COUP-TFI-icKO^Glast* versus *Ctrl^Glast* (Figure S3N). Taken together, these data demonstrate that loss of COUP-TFI in the RGL cell pool severely impairs neurogenesis in the adult DG, without altering NSC/progenitor proliferation and/or newborn cell survival.

Loss of COUP-TFI Function Promotes Astrogliogenic Potential in Adult DG RGL Cells

In addition to neurogenesis, new astrocytes are continuously generated from RGL cells in the adult DG (Bonaguidi et al., 2011; Steiner et al., 2004). We thus hypothesized that the observed reduction of newborn neurons upon *COUP-TFI* inactivation (Figures 3 and S3) could entail increased astrogliogenesis.

(N) Pie charts reporting the fraction of BrdU+YFP+ cells that are DCX+ (dark yellow) at 3 and 17 dpi in C *Ctrl^Glast* and *COUP-TFI-icKO^Glast* DG (3 dpi: n = 142 of 176 cells, *Ctrl^Glast* mice; n = 108 of 207 cells, COUP-TFI-icKOGlast mice; 17 dpi: n = 57 of 68 cells, *Ctrl^Glast* mice; n = 45 of 76 cells, *COUP-TFI-icKO^Glast* mice; Student's t test: p < 0.001 at 3 dpi, p < 0.05 at 17 dpi).
N = 3 or 4 animals per genotype. Arrows indicate double-labeled cells. Scale bars, 50 μm (C, F, H, and J; low magnification), 10 μm (C; high magnification), 25 μm (M; low magnification), and 10 μm (M; high magnification). Error bars indicate SEM. Student's t test: *p < 0.05. See also Figure S3.

For this purpose, we tested the expression of NFIA, a nuclear factor associated with astroglial commitment during development (Kang et al., 2012; Subramanian et al., 2011), in RGL cells and proliferating progenitors of the DG 3 days after TAM-driven recombination (Figures 4A–4D). In *Ctrl*^{Glast} mice, about 60% of all YFP+ RGL cells expressed NFIA (Figure 4B), in a largely mutually exclusive pattern to COUP-TFI (Figures S4A and S4B). This fraction increased to 80% in *COUP-TFI-icKO*^{Glast} mice (Figure 4B). In addition, mutant mice also showed an expansion of MCM2+YFP+ proliferating progenitors expressing NFIA (Figures 4C and 4D). Because no changes in the RGL and proliferative pool cell size were observed (Figures S3F and S3I), these data suggest a switch of COUP-TFI-deficient NSC/progenitor commitment toward an astroglial fate. Accordingly, at this time point, the density of YFP+ astrocytes expressing the mature astroglial marker S100B was comparable between genotypes (Figures S4C and S4D), indicating no direct differentiation of RGL cells into astrocytes.

We next moved to the long-term protocol (Figure 3E) to follow astrocyte differentiation within the YFP+ recombined pool. The majority of YFP+ astrocytes, double-positive for GFAP or S100B, showed cell bodies within the middle/outer GCL and multiple branches reminiscent of a mature astrocyte bushy morphology (Figures 4E and 4F, white arrowheads). Some of the YFP+ astrocytes depicting a polarized shape, but with a thick and short apical process branching mainly inside the GCL, were also identified in the SGZ (Figures 4E and 4F, pink arrowheads). Careful quantification of double GFAP+YFP+ and S100B+YFP+ astrocytes indicated a huge expansion of these cells upon *COUP-TFI* deletion in the Glast lineage (Figures 4G and 4H), which occurred without depletion of the RGL cell pool (Figures S4E and S4F). This suggested that a direct differentiation of RGL cells into astrocytes was unlikely to take place. To evaluate whether astrocytes were derived instead through cell divisions, we analyzed BrdU-injected mice at 17 dpi (Figure 3L) and confirmed a higher percentage of mature astrocytes among the BrdU+YFP+ cells in *COUP-TFI-icKO*^{Glast} DG compared with controls (Figure 4I).

Beside the RGL cell population, we also observed that the *Glast-CreERT2* line triggered recombination in mature astrocytes (expressing Sox2, GFAP, and S100B; Seri et al., 2004; Steiner et al., 2004; Venere et al., 2012), which are scattered in the DG GCL, hilus, and molecular cell layer (MCL), where COUP-TFI is also expressed (Figures S4G and S4H). Thus, *COUP-TFI* depletion in mature astrocytes could directly contribute to the observed increase in DG astrogliogenesis, possibly by "re-awakening" astrocyte proliferative capabilities *in vivo*. We thus checked their ability to re-enter the cell cycle by a short-term BrdU injection protocol (1 dpi) after TAM-dependent recombination (Figure S4I). In both *Ctrl*^{Glast} and *COUP-TFI-icKO*^{Glast} DG, GFAP+YFP+ astrocytes localized in the GCL and MCL failed to incorporate BrdU, and all proliferating cells were confined to the stem cell niche (Figure S4J). In addition, no differences in the density of double GFAP+YFP+ astrocytes were found between mutant and control hippocampal CA1 regions, where normally COUP-TFI is highly expressed (Figures S4K–S4M). Finally, no proliferating Ki67+ astrocytes were also detected (Figure S4N), thus excluding hippocampal mature astrocyte re-activation in *COUP-TFI-icKO*^{Glast} mice.

Overall, these findings indicate that loss of COUP-TFI in RGL cells and their progeny promotes an astrogliogenic fate at the expense of a neurogenic one. Thus, COUP-TFI acts primordially in the fate decision between neuronal and astroglial lineages within adult NSCs/progenitors.

COUP-TFI Is Necessary in Adult DG Progenitors to Promote Neurogenesis by Repressing Astrogliogenesis

To further demonstrate a direct role for COUP-TFI in repressing astroglial fate in the adult DG niche, COUP-TFI function was exclusively deleted in activated NSCs and early committed neurogenic progenitors (type 2a) by taking advantage of the *Ascl1-CreERT2* mouse line (Figures 5A, 5B, S5A, and S5B) (Battiste et al., 2007). Ten days after TAM administration, only rare triple GFAP+Sox2+YFP+ mature astrocytes (Figures 5C and 5E), accounting for less than 3% of the YFP+ population (Table S1), were observed in *Ctrl*^{Ascl1} mice, demonstrating a predominantly neurogenic fate of the Ascl1 lineage. Notably, *COUP-TFI-icKO*^{Ascl1} DG showed a drastic increase in YFP+ *Ascl1*-derived astrocytes (Figures 5D and 5E; Table S1). These cells, unambiguously distinguishable from RGL cells, showed a polarized morphology, with their soma localized mostly in the deep GCL (Figure 5D, left). We also observed some YFP+ astrocytes in the most superficial GCL depicting a mature morphology (Figure 5D, right) and expressing S100B (Figure 5F). A significant decrease in DG YFP+ neuroblasts/immature neurons, both in terms of double DCX+YFP+ cell density and as percentage of DCX+ cells among the YFP+ population, was also assessed in *COUP-TFI-icKO*^{Ascl1} mice compared with control ones (Figures 5G and 5H; Table S1). This indicates that COUP-TFI is necessary to promote neurogenesis by repressing an astroglial fate not only in NSCs but also in neurogenic type2a progenitors.

To further confirm a cell-intrinsic role of COUP-TFI in driving cell fate choice in neurogenic progenitors, we directly targeted mitotically active cells by stereotaxically injecting a retrovirus expressing *Cre-recombinase* (RV-Cre) (Rolando et al., 2016) in the DG of either *Rosa26-YFP;COUP-TFIfl/fl* mice (*cKO*^{RV-Cre}) or, as controls, in the *Rosa26-YFP* reporter line alone (*Ctrl*^{RV-Cre}) (Figures 5I and S5C). Two days after retroviral injection, densities of YFP+ cells were similar in the two genotypes (Figure S5D), while the percentage of double COUP-TFI+YFP+ cells dramatically dropped in *cKO*^{RV-Cre} mice (Figure S5E). At this time, the large majority of YFP+ cells were progenitors/neuroblasts, and there were no differences between *cKO*^{RV-Cre} and *Ctrl*^{RV-Cre} mice (Figure S5F). Remarkably, at longer survival time (i.e., 18 dpi; Figure 5J), we observed an increase in double GFAP+YFP+ astrocytes and an equivalent reduction in double DCX+YFP+ newborn neurons in *cKO*^{RV-Cre} compared with *Ctrl*^{RV-Cre} mice, with no changes in the total amount of YFP+ cells (Figures 5K–5N and S5G). These findings strongly support a direct involvement of COUP-TFI in repressing an astroglial fate in neurogenic progenitors.

Forced COUP-TFI Expression Prevents Astrogliogenesis in the Healthy DG and Rescues Altered Neuron-to-Astrocyte Generation upon Neuroinflammation

To understand whether COUP-TFI is not only necessary but also sufficient to suppress astrogliogenesis in adult
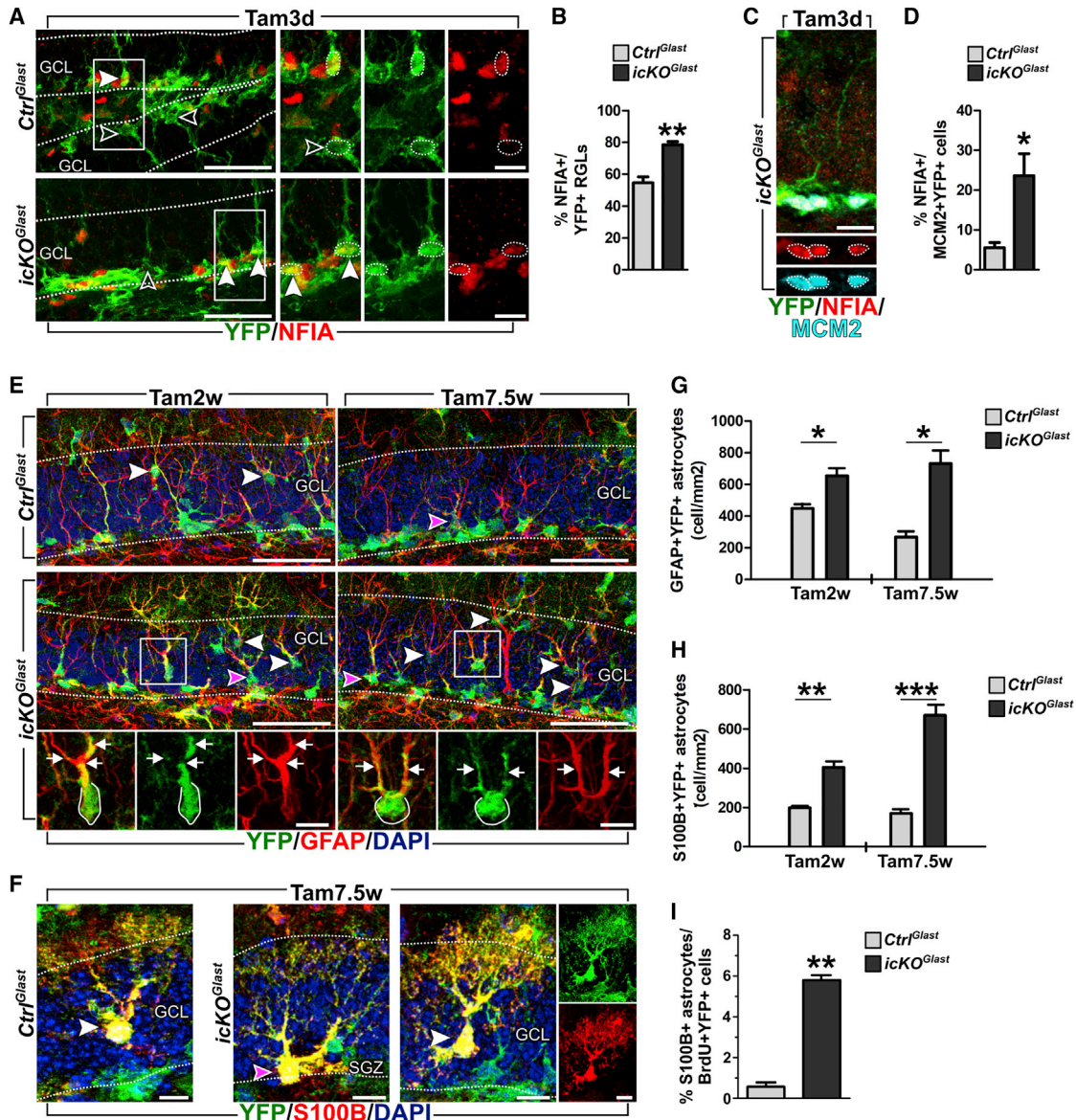
Figure 4. Loss of COUP-TFI Function Promotes Astrogliogenic Potential in Adult DG RGL Cells

(A–D) Refer to experimental strategy shown in Figure 3B.

(A) Confocal images of double immunofluorescence for YFP (green) and NFIA (red) in *Ctrl^Glast* and *COUP-TFI-icKO^Glast* DG. Full arrowheads show double YFP+NFIA+ RGL cells; empty arrowheads show YFP+ RGL cells negative for NFIA.

(B) Quantification of NFIA+ nuclei among YFP+ RGL cells within the GCL/SGZ of *Ctrl^Glast* and *COUP-TFI-icKO^Glast* mice (n = 89 of 162 YFP+ cells in CtrlGlast; n = 90 of 115 YFP+ cells in *COUP-TFI-icKO^Glast*).

(C) Confocal image of triple-labeled YFP (green), NFIA (red), and MCM2 (cyan) cells in *COUP-TFI-icKO^Glast* DG.

(D) Quantification of NFIA+ cells among double MCM2+YFP+ proliferating progenitors within the GCL/SGZ of *Ctrl^Glast* and *COUP-TFI-icKO^Glast* DG (n = 16 of 273 YFP+ cells in *Ctrl^Glast*; n = 54 of 222 YFP+ cells in *COUP-TFI-icKO^Glast*).

(E–H) Refer to experimental strategy shown in Figure 3E.

(E) Confocal images of double GFAP+YFP+ astrocytes in *Ctrl^Glast* and *COUP-TFI-icKO^Glast* DG at Tam2w and Tam7.5w.

(F) Confocal images of mature double S100B+YFP+ astrocytes in *Ctrl^Glast* and *COUP-TFI-icKO^Glast* at Tam7.5w.

(G and H) Quantification of double GFAP+YFP+ (G) and S100B+YFP+ (H) mature astrocytes within the SGZ/GCL in *Ctrl^Glast* and *COUP-TFI-icKO^Glast* at Tam2w and Tam7.5w.

(I) Histogram showing the fraction of newborn S100B+ astrocytes among all BrdU+YFP+ cells within the SGZ/GCL of *Ctrl^Glast* and *COUP-TFI-icKO^Glast* at 17 dpi (refers to protocol in Figure 3L; n = 4 of 198 in *Ctrl^Glast*; n = 15 of 217 in *COUP-TFI-icKO^Glast*).

In (E) and (F), white arrowheads indicate bushy mature astrocytes, while pink arrowheads indicate more polarized astrocytes, whose cell bodies are located in the SGZ. N = 3 or 4 mice/genotype/time point. Error bars indicate SEM. Scale bars, 50 μm (A and E), 10 μm (C), and 10 μm (A and E insets). Student's t test: *p < 0.05, **p < 0.01, and ***p < 0.001. See also Figure S4.
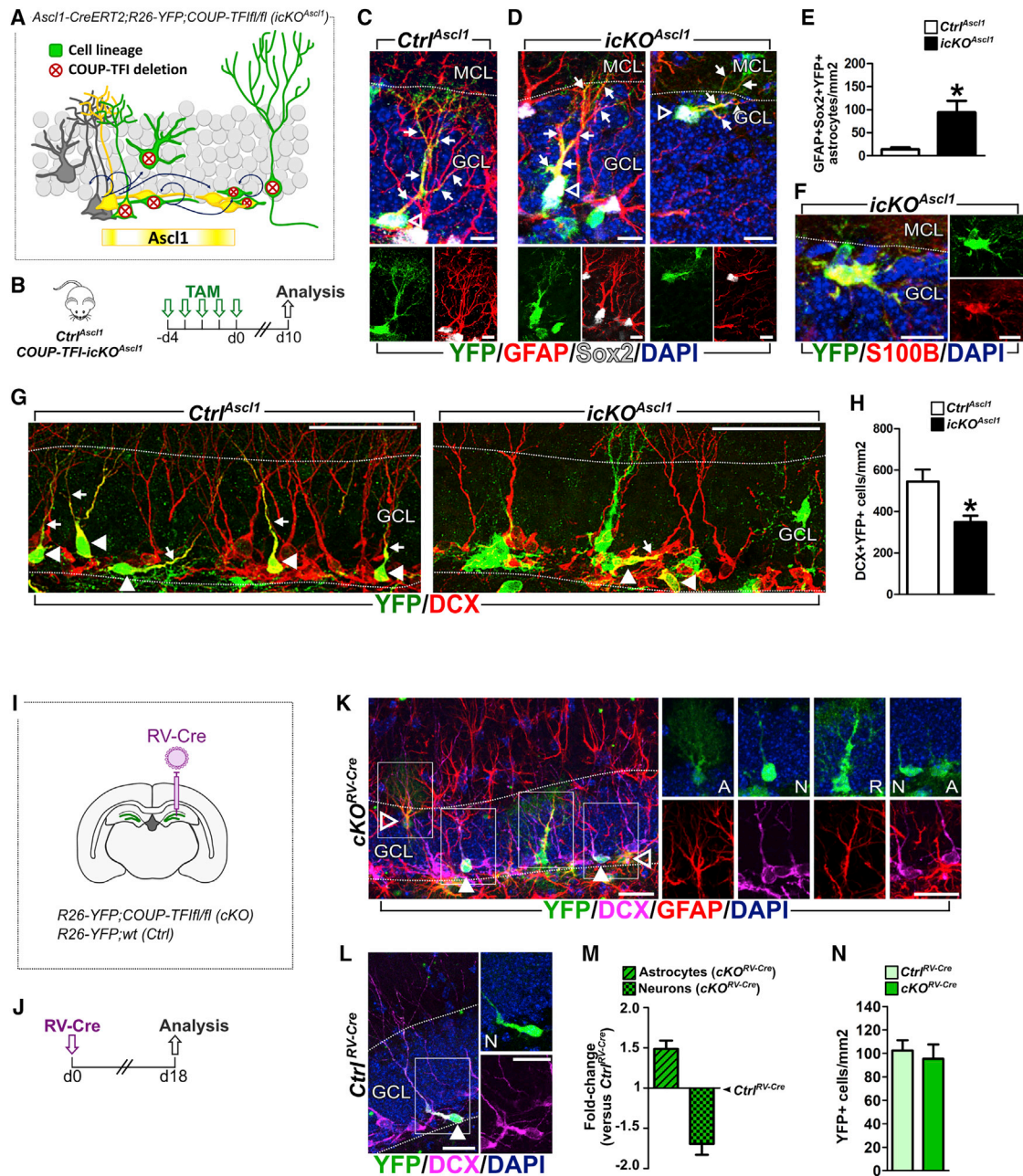
Figure 5. COUP-TFI Is Necessary in Adult DG Progenitors to Promote Neurogenesis by Repressing Astrogliogenesis

(A) Schema illustrating *COUP-TFI* deletion (red crossed circles) in the cell progeny (green) derived from Ascl1-expressing cells (yellow) in the DG upon TAM induction in *COUP-TFI-icKO^Ascl1* mice.

(B) Experimental design to assess the effects of *COUP-TFI* deletion in the Ascl1-lineage (see C–H).

(C and D) Confocal images showing triple GFAP+Sox2+YFP+ newborn astrocytes in the DG of *Ctrl^Ascl1* (C) and *COUP-TFI-icKO^Ascl1* (D) mice. DAPI counterstaining (blue).

(E) Quantification of GFAP+Sox2+YFP+ newborn astrocytes within the SGZ/GCL of *Ctrl^Ascl1* and *COUP-TFI-icKO^Ascl1* DG.

(F) Confocal image of a mature S100B+YFP+ astrocyte in the GCL of *COUP-TFI-icKO^Ascl1* DG.

(G) Confocal images of DG sections stained for DCX (red) and YFP (green) in *Ctrl^Ascl1* and *COUP-TFI-icKO^Ascl1* mice.

(H) Quantification of DCX+YFP+ newborn neurons within the SGZ/GCL of *Ctrl^Ascl1* and *COUP-TFI-icKO^Ascl1* DG.

(I) Experimental strategy used for COUP-TFI loss-of-function in dividing DG neural progenitors by Cre-expressing retrovirus (RV-Cre) stereotaxic injection (see K–N).

(J) Experimental design for RV-Cre injection and analysis of newborn cell phenotype.

NSCs/progenitors, we adopted a gain-of-function approach using *Glast-CreERT2;Rosa26-YFP;lox-stop-lox-hCOUP-TFI* mice (*COUP-TFI-O/E^{Glast}*). In these mice, COUP-TFI is overexpressed in RGL cells and their lineage upon *Cre*-mediated inducible recombination (Figures 6A and S6A) (Alfano et al., 2014; Parisot et al., 2017; Wu et al., 2010). Two weeks after TAM treatment, the density of GFAP+YFP+ astrocytes within the SGZ/GCL of *COUP-TFI-O/E^{Glast}* was reduced by half compared with controls (Figures 6C and 6D; Table S1). This likely reflects impaired astrogliogenesis upon COUP-TFI overexpression. Indeed, while in control animals GFAP+YFP+ astrocytes within the SGZ/GCL doubled between 2 and 14 days after TAM, the density of astrocytes in the *COUP-TFI-O/E^{Glast}* mice at 14 days was comparable with that of controls at 2 days after TAM (Figures S6B–S6D). Moreover, we did not observe changes between genotypes in the total YFP+ population and YFP+ RGL cells (Figures S6E and S6F), as well as in YFP+ astrocytes outside of the DG neurogenic compartment (i.e., MCL; Figure S6G). On the whole, these data point to reduced astrogliogenesis in the presence of high COUP-TFI expression in RGL cells and their progeny.

Neurogenesis did not significantly change in *COUP-TFI-O/E^{Glast}* DG (Figures 6E and 6F). However, we found an increase in the density of caspase-3+NeuroD+YFP+ cells in mutant DG compared with controls, indicating induced apoptosis in newborn neurons that accounted for all DG caspase-3+YFP+ cells (Figures S6H–S6J). Considering high endogenous COUP-TFI protein levels in neuronal progenitors/neuroblasts (Figures 2E and 2F), its forced overexpression might induce an apoptotic pathway within the neuronal lineage.

In light of our previously described COUP-TFI downregulation within the adult DG upon acute LPS-induced neuroinflammation (Figure 1), we finally wondered whether forcing COUP-TFI expression in this condition could prevent enhanced astrogliogenesis and rescue neurogenesis. To this aim, we stereotaxically injected the retrovirus RV-Cre in the DG of adult *COUP-TFI-O/E^{RV-Cre}* and relative controls (*Ctrl^{RV-Cre}*) and treated mice with LPS 1 day later for 4 days (Figures 6G, 6H, and S6K–S6M). Two weeks after RV-Cre injection, we found comparable densities of YFP+ recombined cells within the SGZ/GCL compartment of saline- or LPS-treated *Ctrl^{RV-Cre}* and LPS-treated *COUP-TFI-O/E^{RV-Cre}* mice (Figure 6I). However, LPS-treated *Ctrl^{RV-Cre}* mice showed a 2-fold increase in GFAP+YFP+ astrocytes and a reduction in DCX+YFP+ newborn neurons versus saline-treated *Ctrl^{RV-Cre}* animals (Figures 6J and S6K–S6M). Notably, LPS-induced effects were completely reverted by COUP-TFI gain-of-function (Figures 6J and S6M). Indeed, the percentages of newborn astrocytes and neurons were respectively lower and higher in LPS-treated *COUP-TFI-O/E^{RV-Cre}* mice compared with both LPS- and saline-treated *Ctrl^{RV-Cre}* (Figures S6K and S6L). These data demonstrate that forced

COUP-TFI expression in adult neural progenitors is sufficient to rescue the imbalance in newborn neuron-to-astrocyte ratio during neuroinflammation.

DISCUSSION

The lifelong production and integration of new DG granule neurons are considered an extreme form of plasticity in the adult brain, which contributes to learning and memory (Gonçalves et al., 2016). Adult DG NSCs give rise to newborn neurons, but they also produce astrocytes, whose function and generation are not as well characterized (Bond et al., 2015). The fate choice between a neuron and an astrocyte in NSCs is subject to dynamic modulation through extrinsic signals. Indeed, decreased neurogenesis paralleled by increased generation of astrocytes is a feature observed in mouse models of neuroinflammation (Kohman and Rhodes, 2013); this imbalance could contribute to the inflammation-associated cognitive impairments, possibly by remodeling neural circuits and acting on memory consolidation (Valero et al., 2014). Thus, understanding NSC cell-intrinsic responses to inflammation might be crucial not only to elucidate the mechanisms of how NSCs react to tissue damage but also to shed light on the regulatory functions occurring in physiological conditions.

Although significant progress has been made in understanding extrinsic and intrinsic cues regulating adult NSC activity in vertebrates, little was known on the transcriptional program controlling astroglial versus neuronal fate choice of adult hippocampal NSCs/progenitors. In this study, we unraveled an unexpected role for the transcriptional regulator COUP-TFI in balancing neuro- and astrogliogenesis within the adult DG. First, we showed that this transcription factor is widely expressed in the healthy DG and that its protein level increases from radial NSCs to neuronal committed progenitors/neuroblasts, in accordance with a recent DG single-cell gene expression analysis (Artegiani et al., 2017). Furthermore, through loss- and gain-of-function approaches, we provided evidence that COUP-TFI is both necessary and sufficient to inhibit an astroglial fate and to drive adult NSCs/progenitors toward a neuronal lineage in the hippocampal neurogenic niche. This is supported by the increased expression of the pro-astrogliogenic transcription factor NFIA not only in NSCs but also in mitotically active progenitors of *COUP-TFI-icKO^{Glast}* DG. Moreover, loss of COUP-TFI function directly in DG progenitors prompted these cells to acquire an astroglial fate indicating they might still be multipotent, as also recently suggested (Harris et al., 2018) and need COUP-TFI to restrict their potential to a neuronal fate. We thus hypothesized that the increase in astroglia at the expense of newborn neurons observed in the adult DG upon inflammation could be related to COUP-TFI downregulation. Reduced COUP-TFI levels

(K and L) Confocal images of multiple staining for YFP (green), DCX (magenta), GFAP (red), and DAPI counterstaining (blue) in sections from *COUP-TFI-cKO^{RV-Cre}* (K) and *Ctrl^{RV-Cre}* (L) DG. A, newborn astrocyte; N, newborn neuron; R, RGL cell.

(M) Histogram showing the fold change in densities of newborn GFAP+YFP+ astrocytes (striped pattern) and DCX+YFP+ newborn neurons (checkerboard pattern) within the SGZ/GCL of *COUP-TFI-cKO^{RV-Cre}* mice compared with *Ctrl^{RV-Cre}* mice.

(N) Quantification of total YFP+ cells within the SGZ/GCL of *Ctrl^{RV-Cre}* and *COUP-TFI-cKO^{RV-Cre}* DG. Student's t test: p = 0.6630.

N = 3 or 4 animals per genotype. Empty arrowheads indicate astrocyte cell bodies, full arrowheads indicate neurons and arrows indicate cellular processes. Error bars indicate SEM. MCL, molecular cell layer. Scale bars, 10 μm (C, D, and F), 50 μm (G), and 20 μm (K and L). Student's t test: *p < 0.05. See also Figure S5.
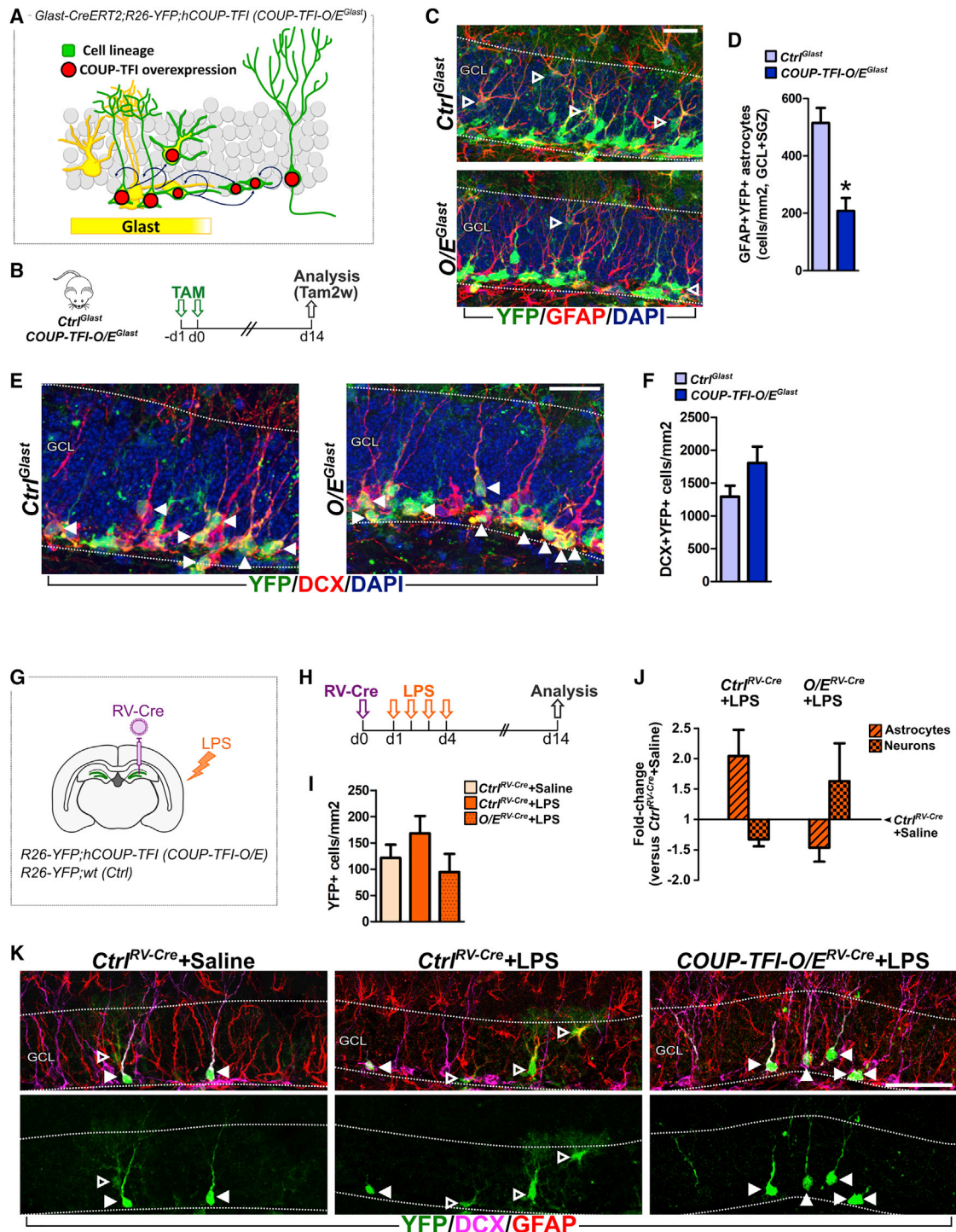
Figure 6. Forced COUP-TFI Expression Prevents Astrogliogenesis in the Healthy DG and Rescues Altered Neuron-Astroglia Generation upon Neuroinflammation

(A) Schema illustrating COUP-TFI overexpression (red circles) in the cell progeny (green) derived from *Glast*-expressing cells (yellow) in the DG upon TAM induction in *COUP-TFI-O/E*^{Glast} adult mice.

(B) Experimental design to assess the effects of COUP-TFI overexpression in the Glast-lineage (see C–F).

(C) Confocal images of DG sections immunostained for YFP (green) and GFAP (red) with DAPI counterstaining (blue) in *Ctrl*^{Glast} and *COUP-TFI-O/E*^{Glast} mice.

(D) Quantification of double GFAP+YFP+ astrocytes within the SGZ/GCL of *Ctrl*^{Glast} and *COUP-TFI-O/E*^{Glast} DG at Tam2w.

(E) Confocal images of DG sections immunostained for YFP (green) and DCX (red) with DAPI counterstaining (blue) in *Ctrl*^{Glast} and *COUP-TFI-O/E*^{Glast} mice.

(legend continued on next page)

would release a normally strong repression of a gliogenic fate in NSCs and progenitors. Indeed, our data showed that forced COUP-TFI expression in mitotically active progenitors is sufficient to prevent LPS-induced astrogliogenesis, revealing a potential role for COUP-TFI in protecting the adult neural niche from inflammatory insults.

The persistence of neurogenesis within the adult brain has been suggested to result from the action of several neurogenic factors counteracting a gliogenic environment (Götz et al., 2016). In this perspective, we propose that COUP-TFI might exert its neurogenic function by cell-intrinsically repressing a "default" astrogliogenic fate within the adult neurogenic niche. A transcriptional repressive role for COUP-TFI has also been described during pallial, subpallial (Alfano et al., 2014; Faedo et al., 2008; Lodato et al., 2011; Tomassy et al., 2010), and eye development (Inoue et al., 2010; Tang et al., 2010) in the mouse, but also in *C. elegans* and *Drosophila* (Mlodzik et al., 1990; Zhou and Walthall, 1998). In this study, we demonstrate that COUP-TFI acts as molecular "sensor" in the adult DG neurogenic niche by responding to external cues and allowing multipotent NSCs/progenitors to take either an astroglial or a neuronal lineage. Understanding how NSCs/progenitors can integrate environmental signals via COUP-TFI and/or other factors, and identifying the molecular pathways downstream of their activity deserves further investigations.

EXPERIMENTAL PROCEDURES

Animals and Treatments

All experiments were performed on 2- to 4-month-old C57BL/6J mice of both genders (Charles River). *Glast-CreERT2+/wt;R26-YFP+/+;COUP-TFIfl/fl* (*COUP-TFI-icKO^{Glast}*), *Glast-CreERT2+/wt;R26-YFP+/+;COUP-TFIwt/wt* (*Ctrl^{Glast}*), *Ascl1-CreERT2+/wt;R26-YFP+/wt;COUP-TFIfl/fl* (*COUP-TFI-icKO^{Ascl1}*), *Ascl1-CreERT2+/−;R26-YFP+/wt;COUP-TFIwt/wt* (*Ctrl^{Ascl1}*), and *Glast-CreERT2+/−;R26-YFP+/+;hCOUP-TFI+/wt* (*COUP-TFI-O/E^{Glast}*) were used for *in vivo* loss- and gain-of-function experiments obtained upon TAM (2.5 mg/mouse/day) administration. Subgroups of these mice also received the thymidine analog 5-bromo-2-deoxyuridine (BrdU; 100 mg/kg; two i.p. injections, 8 hr apart for the 3 and 17 dpi survival experiments, or three i.p. injections, 2 hr apart the day before sacrifice for the proliferation experiment). *R26-YFP+/+;COUP-TFIfl/fl* (*COUP-TFI-cKO^{RV-Cre}*), *R26-YFP+/+;COUP-TFIwt/wt* (*Ctrl^{RV-Cre}*), and *R26-YFP+/+;hCOUP-TFI+/wt* (*COUP-TFI-O/E^{RV-Cre}*) were used for loss- and gain-of-function experiments obtained by RV-Cre stereotaxic injections within the adult DG. For neuroinflammation experiments, mice received *E. coli*-derived LPS (0.5 mg/kg/day) or saline solution (0.9%) as a single i.p. injection for 1 day or 4 consecutive days. Mice were housed under standard laboratory conditions. See the Supplemental Experimental Procedures. All procedures were conducted in accordance with the Guide for the Care and Use of Laboratory Animals of the European Community Council

Directives (2010/63/EU and 86/609/EEC) and approved by local bioethics committees, the Italian Ministry of Health, and the French Ministry for Higher Education and Research.

Tissue Collection, RNA Extraction, and RT-qPCR

Hippocampi from adult mice perfused with ice-cold PBS were microdissected and lysed. RNA isolation, cDNA synthesis, and RT-qPCR were performed according to the manufacturer's instructions. See the Supplemental Experimental Procedures.

Microscope Analysis and Cell Counting

Representative images showing COUP-TFI *in situ* hybridization (ISH) and immunohistochemistry (IHC) were taken on a Nikon microscope coupled to Neurolucida software. Images of double- or triple-immunolabeled sections were acquired using a TCS SP5 confocal microscope (Leica), and multi-stack images were then analyzed with ImageJ (NIH). At least three different levels along the rostro-caudal DG axis were analyzed and cell densities are expressed as cells per square millimeter. See the Supplemental Experimental Procedures.

Statistical Analysis

Statistical comparisons were conducted using two-tailed unpaired Student's t test or one-way ANOVA and the Bonferroni *post-hoc* test when appropriate (in Microsoft Excel and GraphPad Prism5). For unpaired Student's t test, Levene's test was conducted to compare variances, and Welch's correction was applied in case of unequal variance distribution. Significance was established at p < 0.05. Cell counts are presented as mean ± SEM (n ≥ 3 animals per each quantification).

SUPPLEMENTAL INFORMATION

Supplemental Information includes Supplemental Experimental Procedures, six figures, and one table and can be found with this article online at https://doi.org/10.1016/j.celrep.2018.06.044.

(F) Quantification of double DCX+YFP+ neurons within the SGZ/GCL of *Ctrl^{Glast}* and *COUP-TFI-O/E^{Glast}* at Tam2w. Student's t test: p = 0.1619.

(G) Experimental strategy to induce COUP-TFI gain of function in diving neural progenitors by Cre-expressing retrovirus (RV-Cre) stereotaxic injection in LPS-treated mice.

(H) Experimental design for analyzing newborn cell phenotype on inflamed RV-Cre injected *COUP-TFI-O/E* DG.

(I) Quantification of YFP+ cells within the SGZ/GCL of *Ctrl^{RV-Cre}*+Saline, *Ctrl^{RV-Cre}*+LPS, and *COUP-TFI-O/E^{RV-Cre}*+LPS mice. One-way ANOVA: $F_{(2,8)}$ = 1.4546, p = 0.2892, with Bonferroni *post-hoc*-test: *Ctrl^{RV-Cre}*+Saline versus *Ctrl^{RV-Cre}*+LPS versus *COUP-TFI-O/E^{RV-Cre}*+LPS, p > 0.05.

(J) Histogram showing the fold change in densities of newborn GFAP+YFP+ astrocytes (striped pattern) and DCX+YFP+ newborn neurons (checkerboard pattern) within the SGZ/GCL of *Ctrl^{RV-Cre}*+LPS and *COUP-TFI-O/E^{RV-Cre}*+LPS mice normalized to *Ctrl^{RV-Cre}*+Saline.

(K) Confocal images of DG sections immunostained for YFP (green), DCX (magenta), and GFAP (red) in *Ctrl^{RV-Cre}*+Saline, *Ctrl^{RV-Cre}*+LPS, and *COUP-TFI-O/E^{RV-Cre}*+LPS mice.

N = 3 or 4 animals per genotype. Empty arrowheads indicate astrocyte cell bodies and full arrowheads indicate neurons. Error bars indicate SEM. Scale bars, 20 μm (C and E) and 50 μm (K). Student's t test: *p < 0.05. See also Figure S6.

AUTHOR CONTRIBUTIONS

S.B., S.D.M., and M.S. conceptualized and planned the research. W.K. contributed to conceptualizing and planning experiments concerning inflammation. S.B., S.D.M., and I.C. conducted the research. A.P.-D. performed mRNA sampling and RT-qPCR experiments. C.R. provided the RV-Cre. S.B., S.D.M., I.C., and A.P.-D. analyzed data. S.B., S.D.M., and M.S. wrote the paper.

DECLARATION OF INTERESTS

The authors declare no competing interests.

REFERENCES

Al-Kateb, H., Shimony, J.S., Vineyard, M., Manwaring, L., Kulkarni, S., and Shinawi, M. (2013). NR2F1 haploinsufficiency is associated with optic atrophy, dysmorphism and global developmental delay. Am. J. Med. Genet. A. *161A*, 377–381.

Alfano, C., Viola, L., Heng, J.I.-T., Pirozzi, M., Clarkson, M., Flore, G., De Maio, A., Schedl, A., Guillemot, F., and Studer, M. (2011). COUP-TFI promotes radial migration and proper morphology of callosal projection neurons by repressing Rnd2 expression. Development *138*, 4685–4697.

Alfano, C., Magrinelli, E., Harb, K., Hevner, R.F., and Studer, M. (2014). Postmitotic control of sensory area specification during neocortical development. Nat. Commun. *5*, 5632.

Andersen, J., Urbán, N., Achimastou, A., Ito, A., Simic, M., Ullom, K., Martynoga, B., Lebel, M., Göritz, C., Frisén, J., et al. (2014). A transcriptional mechanism integrating inputs from extracellular signals to activate hippocampal stem cells. Neuron *83*, 1085–1097.

Armentano, M., Chou, S.-J., Tomassy, G.S., Leingärtner, A., O'Leary, D.D.M., and Studer, M. (2007). COUP-TFI regulates the balance of cortical patterning between frontal/motor and sensory areas. Nat. Neurosci. *10*, 1277–1286.

Artegiani, B., Lyubimova, A., Muraro, M., van Es, J.H., van Oudenaarden, A., and Clevers, H. (2017). A single-cell RNA sequencing study reveals cellular and molecular dynamics of the hippocampal neurogenic niche. Cell Rep. *21*, 3271–3284.

Barkho, B.Z., Song, H., Aimone, J.B., Smrt, R.D., Kuwabara, T., Nakashima, K., Gage, F.H., and Zhao, X. (2006). Identification of astrocyte-expressed factors that modulate neural stem/progenitor cell differentiation. Stem Cells Dev. *15*, 407–421.

Battiste, J., Helms, A.W., Kim, E.J., Savage, T.K., Lagace, D.C., Mandyam, C.D., Eisch, A.J., Miyoshi, G., and Johnson, J.E. (2007). Ascl1 defines sequentially generated lineage-restricted neuronal and oligodendrocyte precursor cells in the spinal cord. Development *134*, 285–293.

Bertacchi, M., Parisot, J., and Studer, M. (2018). The pleiotropic transcriptional regulator COUP-TFI plays multiple roles in neural development and disease. Brain Res. Published online April 27, 2018. https://doi.org/10.1016/j.brainres.2018.04.024.

Bonaguidi, M.A., Wheeler, M.A., Shapiro, J.S., Stadel, R.P., Sun, G.J., Ming, G.L., and Song, H. (2011). In vivo clonal analysis reveals self-renewing and multipotent adult neural stem cell characteristics. Cell *145*, 1142–1155.

Bond, A.M., Ming, G.L., and Song, H. (2015). Adult mammalian neural stem cells and neurogenesis: five decades later. Cell Stem Cell *17*, 385–395.

Bosch, D.G.M., Boonstra, F.N., Gonzaga-Jauregui, C., Xu, M., de Ligt, J., Jhangiani, S., Wiszniewski, W., Muzny, D.M., Yntema, H.G., Pfundt, R., et al.; Baylor-Hopkins Center for Mendelian Genomics (2014). NR2F1 mutations cause optic atrophy with intellectual disability. Am. J. Hum. Genet. *94*, 303–309.

Bovetti, S., Bonzano, S., Garzotto, D., Giannelli, S.G., Iannielli, A., Armentano, M., Studer, M., and De Marchis, S. (2013). COUP-TFI controls activity-dependent tyrosine hydroxylase expression in adult dopaminergic olfactory bulb interneurons. Development *140*, 4850–4859.

DeCarolis, N.A., Mechanic, M., Petrik, D., Carlton, A., Ables, J.L., Malhotra, S., Bachoo, R., Götz, M., Lagace, D.C., and Eisch, A.J. (2013). In vivo contribution of nestin- and GLAST-lineage cells to adult hippocampal neurogenesis. Hippocampus *23*, 708–719.

Encinas, J.M., Michurina, T.V., Peunova, N., Park, J.-H., Tordo, J., Peterson, D.A., Fishell, G., Koulakov, A., and Enikolopov, G. (2011). Division-coupled astrocytic differentiation and age-related depletion of neural stem cells in the adult hippocampus. Cell Stem Cell *8*, 566–579.

Faedo, A., Tomassy, G.S., Ruan, Y., Teichmann, H., Krauss, S., Pleasure, S.J., Tsai, S.Y., Tsai, M.-J., Studer, M., and Rubenstein, J.L.R. (2008). COUP-TFI coordinates cortical patterning, neurogenesis, and laminar fate and modulates MAPK/ERK, AKT, and beta-catenin signaling. Cereb. Cortex *18*, 2117–2131.

Flore, G., Di Ruberto, G., Parisot, J., Sannino, S., Russo, F., Illingworth, E.A., Studer, M., and De Leonibus, E. (2016). Gradient COUP-TFI expression is required for functional organization of the hippocampal septo-temporal longitudinal axis. Cereb. Cortex *27*, 1629–1643.

Gao, Z., Ure, K., Ables, J.L., Lagace, D.C., Nave, K.-A., Goebbels, S., Eisch, A.J., and Hsieh, J. (2009). Neurod1 is essential for the survival and maturation of adult-born neurons. Nat. Neurosci. *12*, 1090–1092.

Gonçalves, J.T., Schafer, S.T., and Gage, F.H. (2016). Adult neurogenesis in the hippocampus: from stem cells to behavior. Cell *167*, 897–914.

Götz, M., Nakafuku, M., and Petrik, D. (2016). Neurogenesis in the developing and adult brain—similarities and key differences. Cold Spring Harb. Perspect. Biol. *8*, 1–23.

Harris, L., Zalucki, O., Clément, O., Fraser, J., Matuzelski, E., Oishi, S., Harvey, T.J., Burne, T.H.J., Heng, J.I.-T., Gronostajski, R.M., and Piper, M. (2018). Neurogenic differentiation by hippocampal neural stem and progenitor cells is biased by NFIX expression. Development *145*, dev155689.

Inoue, M., Iida, A., Satoh, S., Kodama, T., and Watanabe, S. (2010). COUP-TFI and -TFII nuclear receptors are expressed in amacrine cells and play roles in regulating the differentiation of retinal progenitor cells. Exp. Eye Res. *90*, 49–56.

Kang, P., Lee, H.K., Glasgow, S.M., Finley, M., Donti, T., Gaber, Z.B., Graham, B.H., Foster, A.E., Novitch, B.G., Gronostajski, R.M., and Deneen, B. (2012). Sox9 and NFIA coordinate a transcriptional regulatory cascade during the initiation of gliogenesis. Neuron *74*, 79–94.

Kempermann, G. (2015). Activity dependency and aging in the regulation of adult neurogenesis. Cold Spring Harb. Perspect. Biol. *7*, a018929.

Kempermann, G., Song, H., and Gage, F.H. (2015). Neurogenesis in the adult hippocampus. Cold Spring Harb. Perspect. Biol. *7*, a018812.

Kohman, R.A., and Rhodes, J.S. (2013). Neurogenesis, inflammation and behavior. Brain Behav. Immun. *27*, 22–32.

Llorens-Bobadilla, E., Zhao, S., Baser, A., Saiz-Castro, G., Zwadlo, K., and Martin-Villalba, A. (2015). Single-cell transcriptomics reveals a population of dormant neural stem cells that become activated upon brain injury. Cell Stem Cell *17*, 329–340.

Lodato, S., Tomassy, G.S., De Leonibus, E., Uzcategui, Y.G., Andolfi, G., Armentano, M., Touzot, A., Gaztelu, J.M., Arlotta, P., Menendez de la Prida, L., and Studer, M. (2011). Loss of COUP-TFI alters the balance between caudal ganglionic eminence- and medial ganglionic eminence-derived cortical interneurons and results in resistance to epilepsy. J. Neurosci. *31*, 4650–4662.

Lugert, S., Basak, O., Knuckles, P., Haussler, U., Fabel, K., Götz, M., Haas, C.A., Kempermann, G., Taylor, V., and Giachino, C. (2010). Quiescent and active hippocampal neural stem cells with distinct morphologies respond selectively to physiological and pathological stimuli and aging. Cell Stem Cell *6*, 445–456.

Lugert, S., Vogt, M., Tchorz, J.S., Müller, M., Giachino, C., and Taylor, V. (2012). Homeostatic neurogenesis in the adult hippocampus does not involve amplification of Ascl1(high) intermediate progenitors. Nat. Commun. *3*, 670.

Ming, G.L., and Song, H. (2005). Adult neurogenesis in the mammalian central nervous system. Annu. Rev. Neurosci. *28*, 223–250.

Mlodzik, M., Hiromi, Y., Weber, U., Goodman, C.S., and Rubin, G.M. (1990). The Drosophila seven-up gene, a member of the steroid receptor gene superfamily, controls photoreceptor cell fates. Cell *60*, 211–224.

Monje, M.L., Toda, H., and Palmer, T.D. (2003). Inflammatory blockade restores adult hippocampal neurogenesis. Science *302*, 1760–1765.

Mori, T., Tanaka, K., Buffo, A., Wurst, W., Kühn, R., and Götz, M. (2006). Inducible gene deletion in astroglia and radial glia—a valuable tool for functional and lineage analysis. Glia *54*, 21–34.

Naka, H., Nakamura, S., Shimazaki, T., and Okano, H. (2008). Requirement for COUP-TFI and II in the temporal specification of neural stem cells in CNS development. Nat. Neurosci. *11*, 1014–1023.

Naka-Kaneda, H., Nakamura, S., Igarashi, M., Aoi, H., Kanki, H., Tsuyama, J., Tsutsumi, S., Aburatani, H., Shimazaki, T., and Okano, H. (2014). The miR-17/106-p38 axis is a key regulator of the neurogenic-to-gliogenic transition in developing neural stem/progenitor cells. Proc. Natl. Acad. Sci. U S A *111*, 1604–1609.

Parisot, J., Flore, G., Bertacchi, M., and Studer, M. (2017). COUP-TFI mitotically regulates production and migration of dentate granule cells and modulates hippocampal CXCR4 expression. Development *144*, 2045–2058.

Rolando, C., Erni, A., Grison, A., Beattie, R., Engler, A., Gokhale, P.J., Milo, M., Wegleiter, T., Jessberger, S., and Taylor, V. (2016). Multipotency of adult hippocampal NSCs in vivo is restricted by Drosha/NFIB. Cell Stem Cell *19*, 653–662.

Seri, B., García-Verdugo, J.M., Collado-Morente, L., McEwen, B.S., and Alvarez-Buylla, A. (2004). Cell types, lineage, and architecture of the germinal zone in the adult dentate gyrus. J. Comp. Neurol. *478*, 359–378.

Song, H., Stevens, C.F., and Gage, F.H. (2002). Astroglia induce neurogenesis from adult neural stem cells. Nature *417*, 39–44.

Srinivas, S., Watanabe, T., Lin, C.S., William, C.M., Tanabe, Y., Jessell, T.M., and Costantini, F. (2001). Cre reporter strains produced by targeted insertion of EYFP and ECFP into the ROSA26 locus. BMC Dev. Biol. *1*, 4.

Steiner, B., Kronenberg, G., Jessberger, S., Brandt, M.D., Reuter, K., and Kempermann, G. (2004). Differential regulation of gliogenesis in the context of adult hippocampal neurogenesis in mice. Glia *46*, 41–52.

Steiner, B., Klempin, F., Wang, L., Kott, M., Kettenmann, H., and Kempermann, G. (2006). Type-2 cells as link between glial and neuronal lineage in adult hippocampal neurogenesis. Glia *54*, 805–814.

Subramanian, L., Sarkar, A., Shetty, A.S., Muralidharan, B., Padmanabhan, H., Piper, M., Monuki, E.S., Bach, I., Gronostajski, R.M., Richards, L.J., and Tole, S. (2011). Transcription factor Lhx2 is necessary and sufficient to suppress astrogliogenesis and promote neurogenesis in the developing hippocampus. Proc. Natl. Acad. Sci. U S A *108*, E265–E274.

Tang, K., Xie, X., Park, J.-I., Jamrich, M., Tsai, S., and Tsai, M.-J. (2010). COUP-TFs regulate eye development by controlling factors essential for optic vesicle morphogenesis. Development *137*, 725–734.

Tomassy, G.S., De Leonibus, E., Jabaudon, D., Lodato, S., Alfano, C., Mele, A., Macklis, J.D., and Studer, M. (2010). Area-specific temporal control of corticospinal motor neuron differentiation by COUP-TFI. Proc. Natl. Acad. Sci. U S A *107*, 3576–3581.

Valero, J., Mastrella, G., Neiva, I., Sánchez, S., and Malva, J.O. (2014). Longterm effects of an acute and systemic administration of LPS on adult neurogenesis and spatial memory. Front. Neurosci. *8*, 83.

Venere, M., Han, Y.-G., Bell, R., Song, J.S., Alvarez-Buylla, A., and Blelloch, R. (2012). Sox1 marks an activated neural stem/progenitor cell in the hippocampus. Development *139*, 3938–3949.

Woodbury, M.E., Freilich, R.W., Cheng, C.J., Asai, H., Ikezu, S., Boucher, J.D., Slack, F., and Ikezu, T. (2015). miR-155 is essential for inflammation-induced hippocampal neurogenic dysfunction. J. Neurosci. *35*, 9764–9781.

Wu, S.-P., Lee, D.-K., Demayo, F.J., Tsai, S.Y., and Tsai, M.-J. (2010). Generation of ES cells for conditional expression of nuclear receptors and coregulators in vivo. Mol. Endocrinol. *24*, 1297–1304.

Wu, M.D., Hein, A.M., Moravan, M.J., Shaftel, S.S., Olschowka, J.A., and O'Banion, M.K. (2012). Adult murine hippocampal neurogenesis is inhibited by sustained IL-1β and not rescued by voluntary running. Brain Behav. Immun. *26*, 292–300.

Zhou, H.M., and Walthall, W.W. (1998). UNC-55, an orphan nuclear hormone receptor, orchestrates synaptic specificity among two classes of motor neurons in Caenorhabditis elegans. J. Neurosci. *18*, 10438–10444.
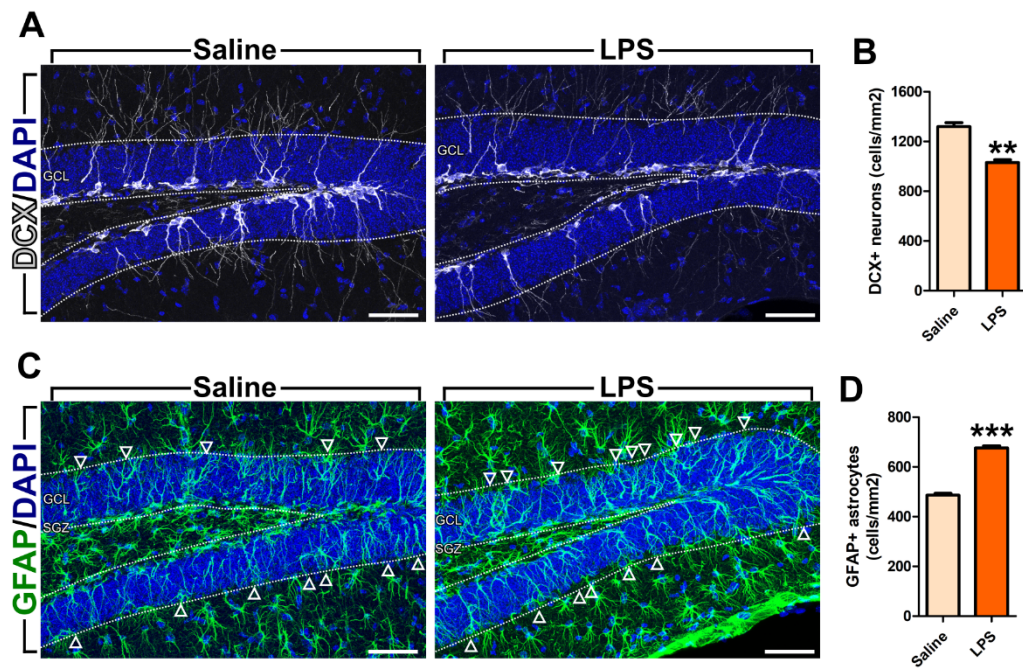
Supplemental Information

Neuron-Astroglia Cell Fate Decision in the Adult

Mouse Hippocampal Neurogenic Niche Is

Cell-Intrinsically Controlled by COUP-TFI *In Vivo*

Sara Bonzano, Isabella Crisci, Anna Podlesny-Drabiniok, Chiara Rolando, Wojciech Krezel, Michèle Studer, and Silvia De Marchis

Figure S1. Reduced newborn neurons and increased astrocytes in the inflamed DG. Related to Figure 1.

(**A**) Confocal images of DCX+ (white) cells in in the DG of saline (control) and LPS-treated mice.

(**B**) DCX+ cell density in the DG of LSP-treated mice *versus* saline.
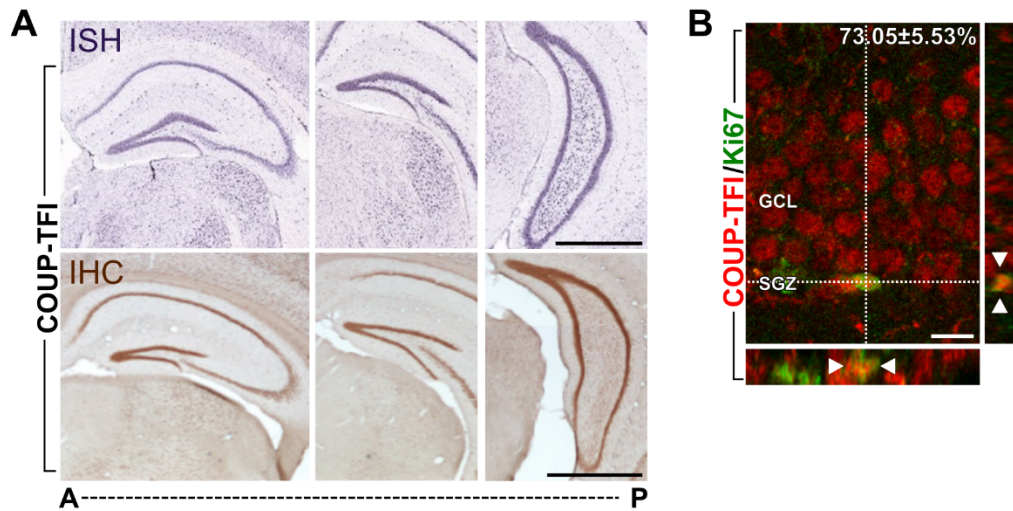
(**C**) Confocal images of GFAP+ (green) cells in the DG of saline and LPS-treated mice. Arrowheads show mature-shaped astrocytes.

(**D**) GFAP+ astrocyte density in the DG of LPS-treated mice *versus* saline.

N=3 mice/treatment. Cell nuclei are counterstained with DAPI (blue). GCL, granule cell layer; SGZ, subgranular zone. Scale bars: A,C, 50µm. Student's t-test **p<0.01, ***p<0.001.

Figure S2. COUP-TFI is widely expressed in the adult DG. Related to Figure 2.

(**A**) Representative images of coronal sections processed for *in situ* hybridization (ISH, top) and immunohistochemistry (IHC, bottom) showing COUP-TFI mRNA and protein expression within the adult hippocampus along its antero (A) - posterior (P) extension. The far right IHC image is a montage.

(**B**) Confocal image of a cell double-labeled for COUP-TFI (red) and Ki67 (green) located in the SGZ of the adult DG. The percentage±SEM of COUP-TFI+ cells expressing the proliferating marker Ki67 (neural stem/progenitor cells) within the adult DG (n=50 cells; N=3 adult mice) are shown (top right). GCL, granule cell layer; SGZ, subgranular zone. Scale bars: A, 1mm; B, 10μm.
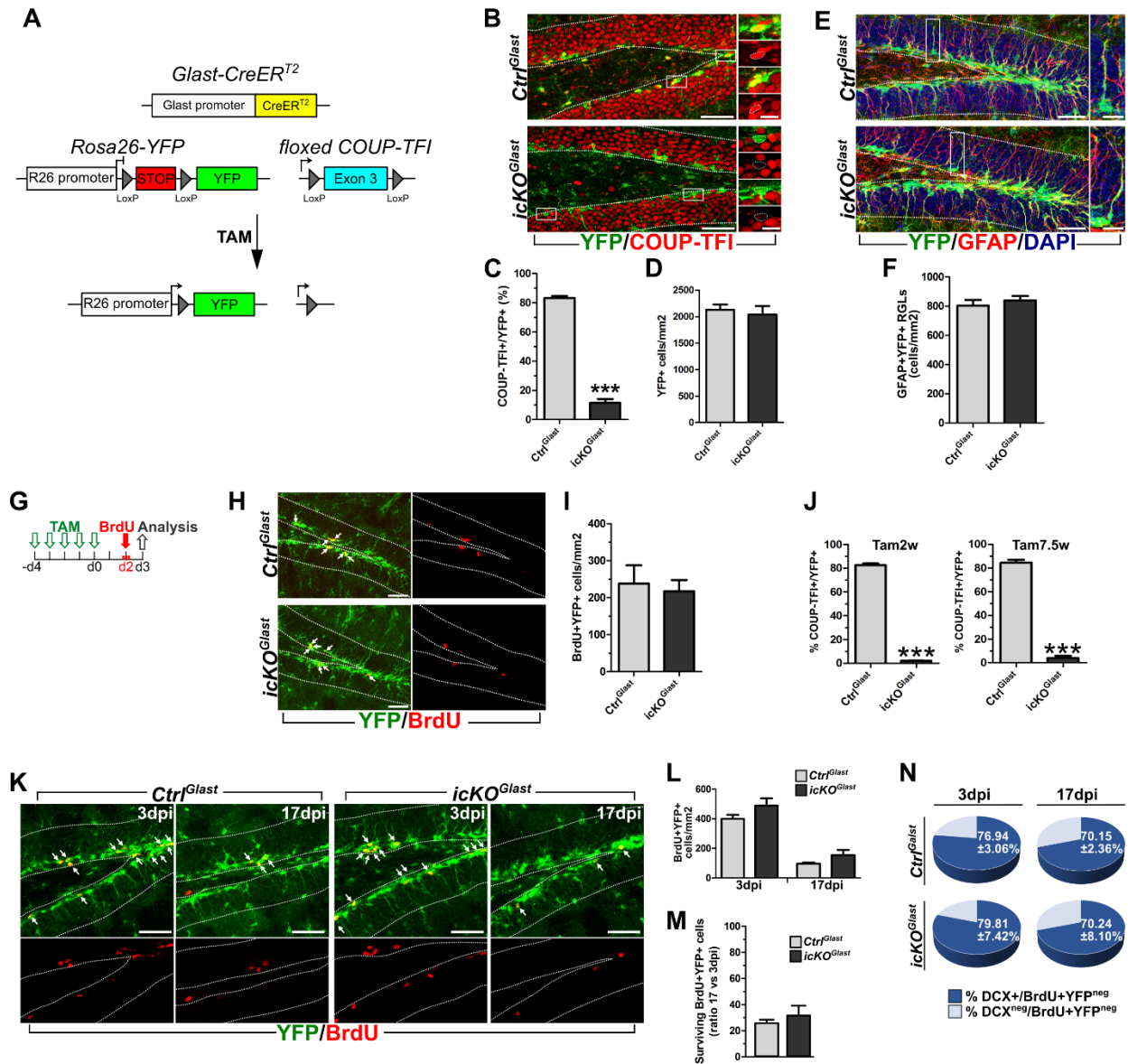
Figure S3. COUP-TFI depletion in adult RGL cells impairs DG neurogenesis. Related to Figure 3.

(**A**) Overview of the Glast-CreERT2, Rosa26-YFP and floxed COUP-TFI alleles and Cre-mediated gene rearrangements.

(**B-F**) Refer to experimental strategy shown in Fig.3B.

(**B**) Confocal images of DG sections immunostained for YFP (green) and COUP-TFI (red) in *Ctrl^Glast* and *COUP-TFI-icKO^Glast* mice.

(**C**) Quantification of COUP-TFI+ cells among YFP+ cells within the GCL/SGZ of *Ctrl^Glast* and *COUP-TFI-icKO^Glast* mice (n=498/597 YFP+ cells in *Ctrl^Glast*; n=92/782 YFP+ cells in *COUP-TFI-icKO^Glast*).

(**D**) Quantification of YFP+ cells within the SGZ/GCL of *Ctrl^Glast* and *COUP-TFI-icKO^Glast* DG. Student's t-test: p=0.6719.

(**E**) Confocal images of DG sections stained for YFP (green), GFAP (red), DAPI (blue) in *Ctrl^Glast* and *COUP-TFI-icKO^Glast* DG.

(**F**) Quantification of GFAP+ RGL cells within the DG of $Ctrl^{Glast}$ and $COUP\text{-}TFI\text{-}icKO^{Glast}$ mice. Student's t-test: p=0.5101.

(**G**) Experimental design to assess the effects of COUP-TFI loss-of-function on proliferation in the Glast-lineage by injecting BrdU (1 day of chase; see H,I).

(**H**) Confocal images of DG sections stained for YFP (green) and BrdU (red) in $Ctrl^{Glast}$ and $COUP\text{-}TFI\text{-}icKO^{Glast}$.

(**I**) Quantification of double BrdU+YFP+ cell density in $Ctrl^{Glast}$ compared to $COUP\text{-}TFI\text{-}icKO^{Glast}$ DG. Student's t-test: p=0.7456.

(**J**) Quantification of COUP-TFI+ nuclei among YFP+ cells within the GCL/SGZ of $Ctrl^{Glast}$ and $COUP\text{-}TFI\text{-}icKO^{Glast}$ animals (refers to protocol Fig. 3E; Tam2w: n=274/332 YFP+ cells in $Ctrl^{Glast}$ mice; n=7/325 YFP+ cells in $COUP\text{-}TFI\text{-}icKO^{Glast}$ mice; Tam7.5w: n=212/250 YFP+ cells in $Ctrl^{Glast}$ mice; n=12/221 YFP+ cells in $COUP\text{-}TFI\text{-}icKO^{Glast}$ mice).

(**K-N**) Refer to experimental strategy shown in Fig. 3L.

(**K**) Confocal images of DG sections stained for YFP+ (green) and BrdU (red) in $Ctrl^{Glast}$ and $COUP\text{-}TFI\text{-}icKO^{Glast}$ DG at 3 days and 17 days post BrdU injection (dpi).

(**L**) Quantification of double-labeled BrdU+YFP+ cells in $Ctrl^{Glast}$ and $COUP\text{-}TFI\text{-}icKO^{Glast}$ DG at 3 dpi and at 17 dpi. Student's t-test: p=0.1924 (3dpi); p=0.1816 (17dpi).

(**M**) Ratio of BrdU+YFP+ cells that survived at 17dpi compared to those at 3dpi in $Ctrl^{Glast}$ and $COUP\text{-}TFI\text{-}icKO^{Glast}$ DG. Student's t-test: p=0.9782.

(**N**) Pie charts reporting the fraction of BrdU+ cells negative for YFP (BrdU+YFP^{neg} cells) co-labeled for DCX+ at 3 dpi and at 17 dpi in $Ctrl^{Glast}$ and $COUP\text{-}TFI\text{-}icKO^{Glast}$ DG (3 dpi: n=98/128 cells in $Ctrl^{Glast}$ mice; n=124/158 cells in $COUP\text{-}TFI\text{-}icKO^{Glast}$ mice, Student's t-test p=0.7471; 17 dpi: n=76/108 cells in 3 $Ctrl^{Glast}$ mice; n=81/114 cells in $COUP\text{-}TFI\text{-}icKO^{Glast}$ mice, Student's t-test p=0.9922).

N=3 mice/genotype. Arrows indicate double-labelled cells. Error bars indicate SEM. Scale bars: B,E,H,K, 50µm; insets, 10µm. Student's t-test: ***p<0.001.
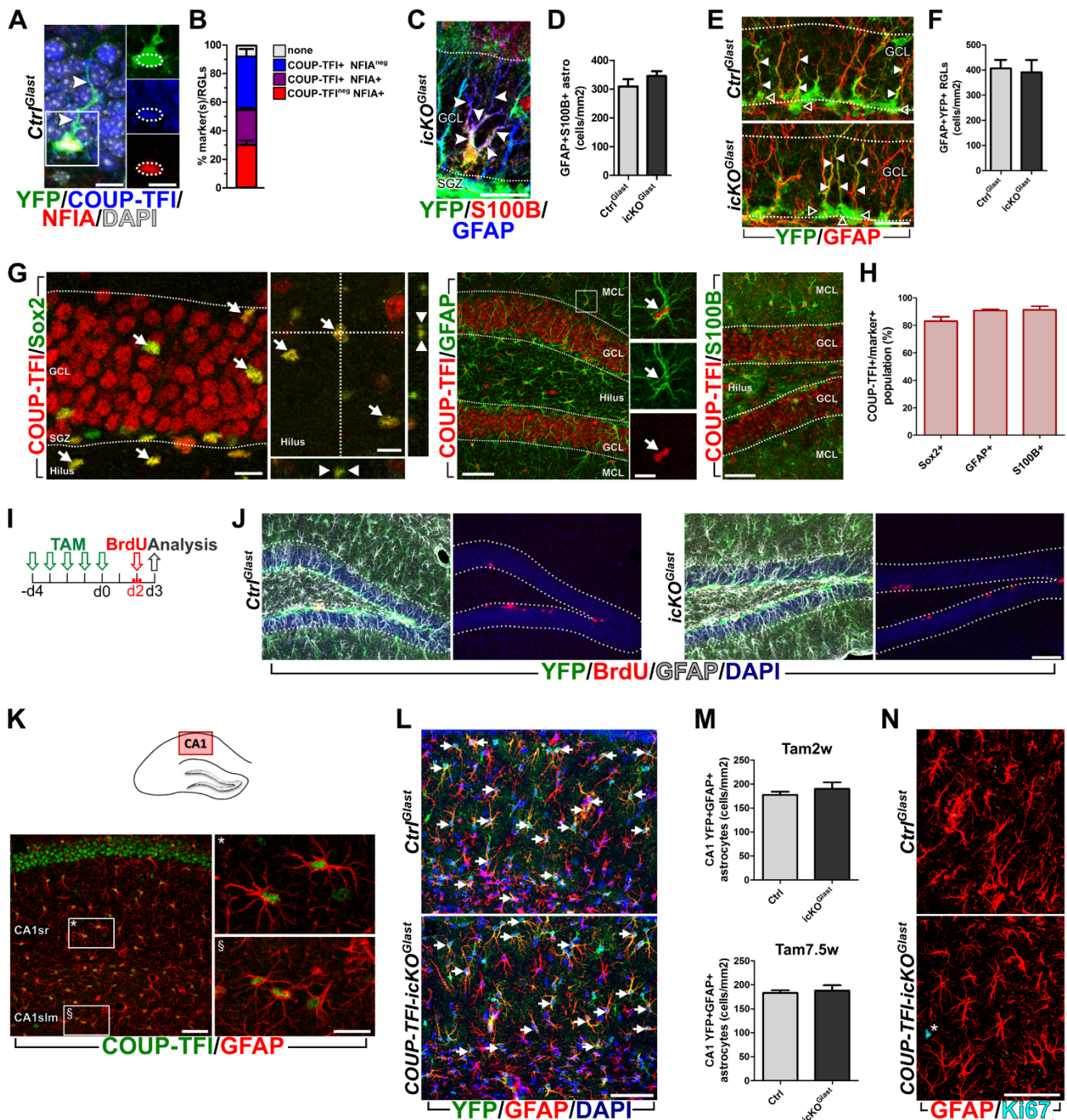
Figure S4. Loss of COUP-TFI function does not induce RGL cell exhaustion or "re-awakening" of mature parenchymal astrocytes. Related to Figure 4.

(**A-D**) Refer to experimental strategy shown in Fig.3B.

(**A**) Confocal image showing a RGL cell triple labeled for COUP-TFI (blue), NFIA (red) and YFP (green) in *Ctrl*[Glast] DG. Arrowheads show the apical radial process.

(**B**) Histogram showing the fraction of single COUP-TFI+ (blue), single NFIA+ (red) or double COUP-TFI+NFIA+ (purple) cells among all YFP+ (green) RGL cells in *Ctrl*[Glast] mice.

(**C**) Confocal image showing an astrocyte triple labeled for S100B (red), GFAP (blue) and YFP (green) in *COUP-TFI-icKO*[Glast] DG. Arrowheads indicate cell processes.

(**D**) Quantification of triple-labeled GFAP+S100B+YFP+ mature astrocytes in *COUP-TFI-icKO*^{Glast} and *Ctrl*^{Glast} DG. Student's t-test: p=0.3179.

(**E,F**) Refer to experimental strategy shown in Fig.3E (Tam2w).

(**E**) Confocal images showing RGL cells double labeled for YFP (green) and GFAP (red) in *COUP-TFI-icKO*^{Glast} and *Ctrl*^{Glast} DG at Tam2w. Note the RGL cell soma in the SGZ (empty arrowheads) and a single thin apical process spanning throughout the GCL (full arrowheads).

(**F**) Quantification of double GFAP+YFP+ RGL cells in the DG of *Ctrl*^{Glast} and *COUP-TFI-icKO*^{Glast} mice at Tam2w. Student's t-test p=0.8953.

(**G**) Confocal images of DG sections from adult wt mice showing double labeling for COUP-TFI (red) and different markers expressed by mature astrocytes (i.e. Sox2, GFAP and S100B; green). Arrows indicate double-labeled cells.

(**H**) Quantification of mature astrocytes labeled by Sox2, GFAP or S100B double positive for COUP-TFI (for each marker, 100 to 200 cells per adult wt mice were analyzed).

(**I**) Experimental design to assess the effects of COUP-TFI loss-of-function on proliferation in the Glast lineage by injecting BrdU (1 dpi).

(**J**) Confocal images of DG sections labeled for YFP (green), BrdU (red) and GFAP (gray) with DAPI counterstaining (blue) following protocol in I.

(**K**) Schematic drawing of a coronal view of the hippocampus and confocal images showing COUP-TFI+ nuclei (green) in GFAP-expressing astrocytes (red) in the adult hippocampal CA1 region.

(**L,N**) Refer to experimental strategy shown in Fig.3E.

(**L**) Confocal images showing YFP (green) and GFAP (red) staining in the hippocampal CA1 of *Ctrl*^{Glast} and *COUP-TFI-icKO*^{Glast} at Tam2w. DAPI counterstaining in blue. Arrows indicate double GFAP+YFP+ astrocytes.

(**M**) Quantification of GFAP+ astrocytes double-labeled for YFP in *Ctrl*^{Glast} and *COUP-TFI-icKO*^{Glast} CA1 region at Tam2w and Tam7.5w (Student's t-test: Tam2w, p=0.4602; Tam7.5w, p=0.7260).

(**N**) Confocal images showing immunofluorescence for GFAP (red) and Ki67 (cyan) in the CA1 region of *Ctrl*^{Glast} and *COUP-TFI-icKO*^{Glast} mice. None of the mature astrocytes analyzed were positive for Ki67 (n=0/2350 GFAP+YFP+ cells in *Ctrl*^{Glast}; n=0/2487 GFAP+YFP+ cells in *COUP-TFI-icKO*^{Glast} DG). Asterisk in the bottom panel highlights a Ki67+ cell negative for GFAP.

N=3/4 animals per genotype. GCL, granule cell layer; MCL, molecular cell layer; SGZ, subgranular zone. Error bars indicate SEM. Scale bars: A,10µm; C,20µm; E, 25µm, G, 10µm (left and insets), 50µm (middle, right-low magnification); J,K,L,N, 50µm (low magnification), 10µm (insets in K).
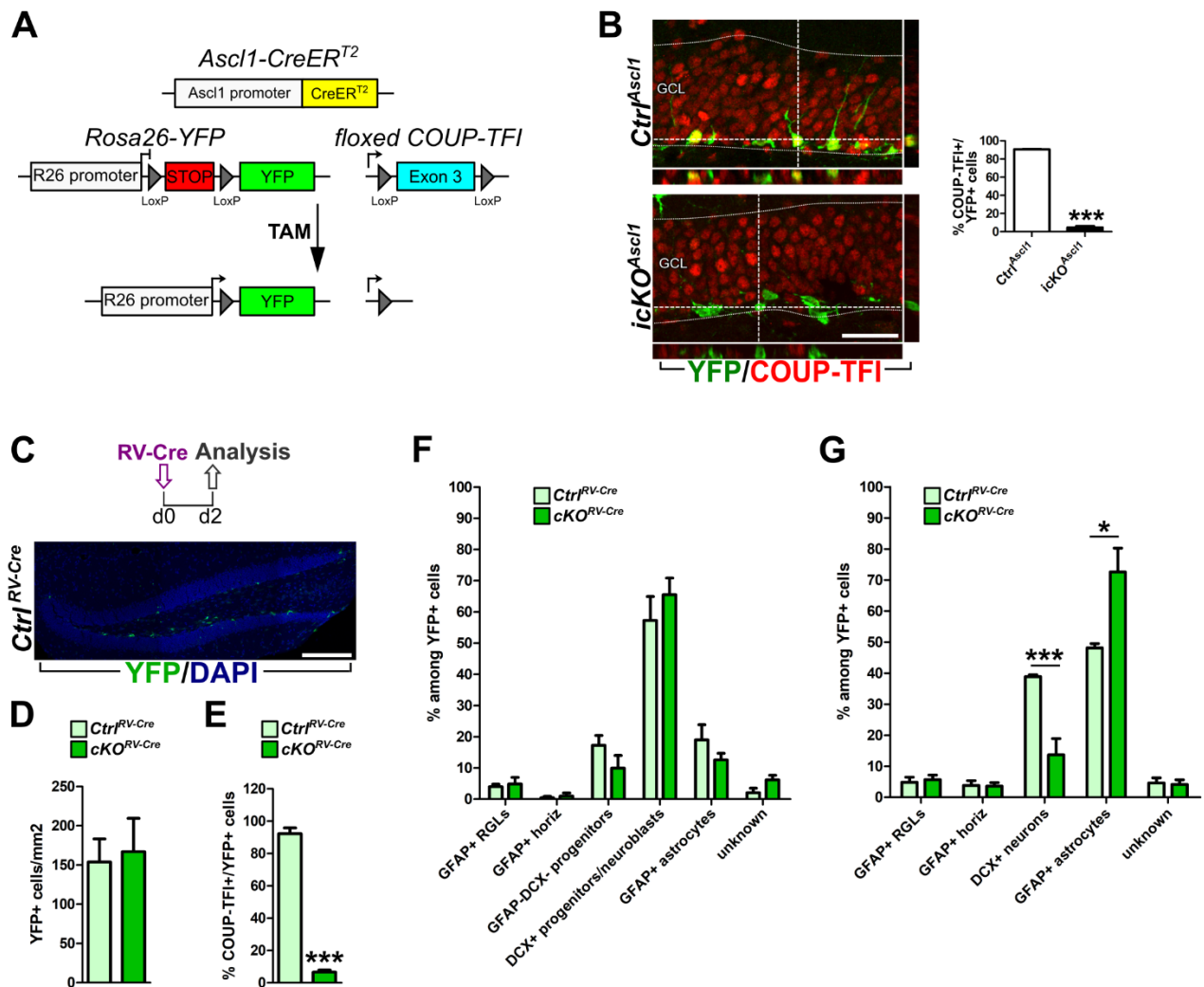
Figure S5. COUP-TFI deletion in adult DG neurogenic progenitors impairs neurogenesis and increases astrogliogenesis. Related to Figure 5.

(**A**) Overview of the Ascl1-CreERT2, Rosa26-YFP and floxed COUP-TFI alleles and Cre-mediated gene rearrangements.

(**B**) Left: confocal images of DG sections immunostained for YFP (green) and COUP-TFI (red) in *Ctrl^{Ascl1}* and *COUP-TFI-icKO^{Ascl1}* mice following the protocol in Fig. 5B (Tam10d). Right: quantification of COUP-TFI+ cells among YFP+ cells within the GCL/SGZ of *Ctr^{tAscl1}* and *COUP-TFI-icKO^{Ascl1}* DG (n=238/263 YFP+ cells in *Ctrl^{Ascl1}*; n=15/332 YFP+ cells in *COUP-TFI-icKO^{Ascl1}*).

(**C**) Short RV-Cre injection protocol (analysis at 2dpi in D-F). Confocal image showing YFP + (green) cells recombined following RV-Cre injection in a DG section counterstaind with DAPI (blue).

(**D**) Quantification of YFP+ cells in *COUP-TFI-cKO^{RV-Cre}* and *Ctrl^{RV-Cre}* DG (2dpi).

(**E**) Quantification of COUP-TFI+ nuclei among YFP+ cells in *COUP-TFI-cKO^{RV-Cre}* and *Ctrl^{RV-Cre}* DG at 2dpi (E; n=125/136 in *Ctrl^{RV-Cre}* and n=8/130 in *COUP-TFI-cKO^{RV-Cre}*).

(**F,G**) Histograms reporting quantification of different cell phenotypes among YFP+ cells in both *Ctrl^{RV-Cre}* and *COUP-TFI-cKO^{RV-Cre}* DG at 2 dpi (F) and 18dpi (G and refers to protocol in Fig. 5J).

N=3/4 animals per genotype. Error bars indicate SEM. GCL, granule cell layer. Scale bars: B, 50µm; C, 100µm; Student's t-test *p<0.05, ***p<0.001.
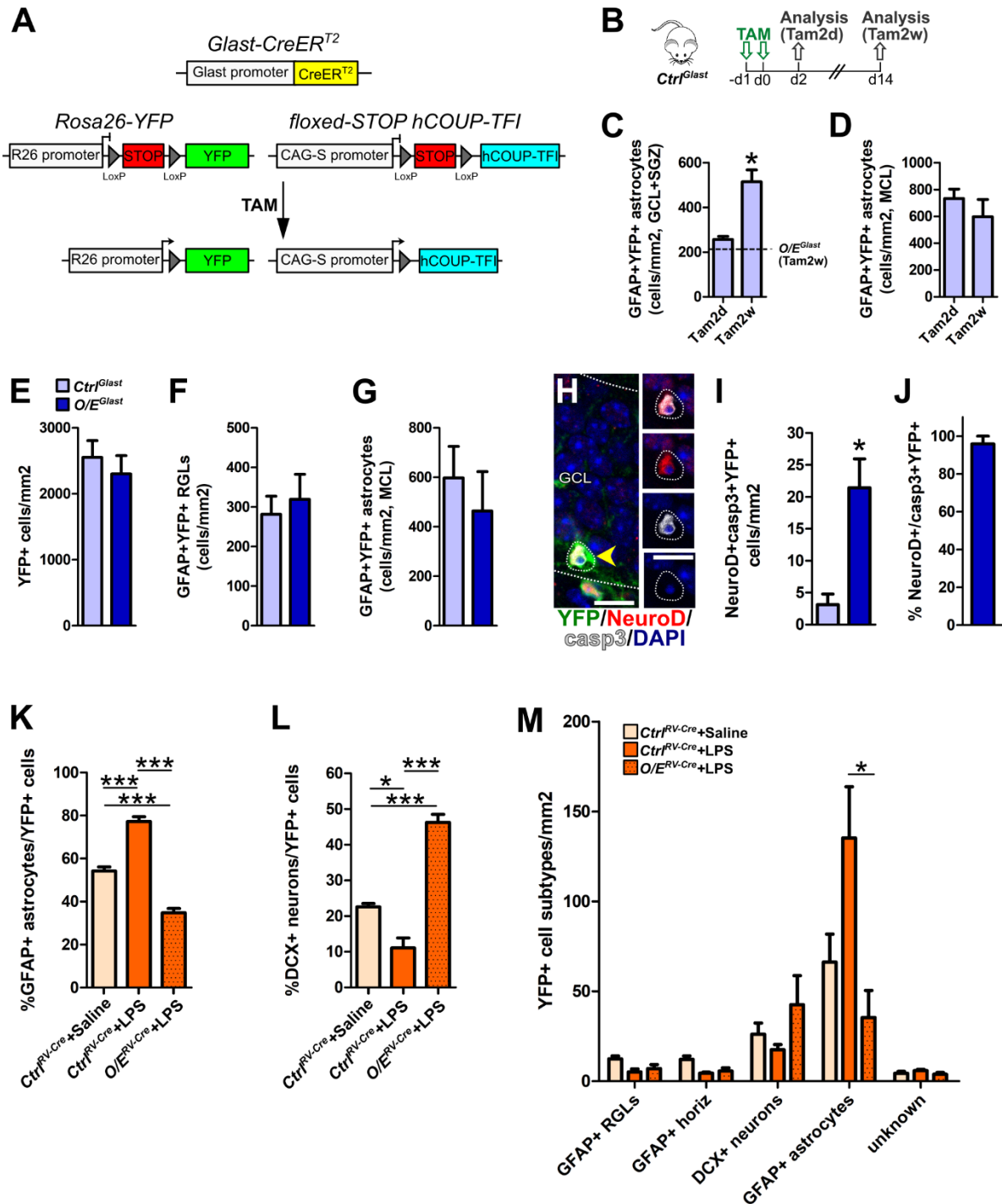
Figure S6. Effects of forced COUP-TFI expression the healthy and inflamed DG. Related to Figure 6.

(**A**) Overview of the Glast-CreERT2, Rosa26-YFP and floxed stop-hCOUP-TFI allele and Cre-mediated gene rearrangements.

(**B**) Experimental design for analysis (see C,D) of recombined YFP+GFAP+ astrocytes in the DG of control mice at 2 days (Tam2d) and 2 weeks (Tam2w) post TAM treatment .

(**C**) Densities of double GFAP+YFP+ astrocytes at Tam2d versus Tam2w in *Ctrl*^{Glast} DG. The dotted line shows density of GFAP+YFP+ astrocytes at Tam2w in *COUP-TFI-O/E*^{Glast} mice.

(**D**) Quantification of double GFAP+YFP+ astrocytes at Tam2d *versus* Tam2w in *Ctrl*^{Glast} MCL shows no differences supporting a specific expansion of the astroglia within the SGZ/GCL at Tam2w.

(**E,F,G**) Quantification of the YFP+ cell pool within the SGZ/GCL (E; Student's t-test p=0.5403), GFAP+YFP+ RGL cells within the SGZ/GCL (F; Student's t-test p=0.2135), and GFAP+YFP+ mature astrocytes within the MCL (G; Student's t-test p=0.5458) in *COUP-TFI-O/E^{Glast}* and *Ctrl^{Glast}* DG.

(**H**) Confocal image of a NeuroD+ (red) YFP+(green) newborn cell also positive for activated-caspase 3 (casp3, gray) in *COUP-TFI-O/E^{Glast}* DG.

(**I**) Quantification of apoptotic newborn neuronal cells (triple-labelled for NeuroD, casp3 and YFP) in *COUP-TFI-O/E^{Glast}* and *Ctrl^{Glast}* DG.

(**J**) Quantification of NeuroD+ nuclei among apoptotic casp3+YFP+ cells in *COUP-TFI-O/E^{Glast}* mice show that almost all apoptotic cells belongs to the neuronal lineage.

(**K,L,M**) refers to experimental design shown in Fig.6H.

(**K**) Quantification of GFAP+ newborn astrocytes on the YFP cell pool within the SGZ/GCL in *Ctrl^{RV-Cre}*+Saline, *Ctrl^{RV-Cre}*+LPS, and *COUP-TFI-O/E^{RV-Cre}*+LPS DG at 14dpi (one-way ANOVA F$_{(2;8)}$= 96.83, p<0.0001 followed by Bonferroni post hoc test)

(**L**) Quantification of DCX+ newborn neurons on the YFP cell pool within the SGZ/GCL in *Ctrl^{RV-Cre}*+Saline, *Ctrl^{RV-Cre}*+LPS, and *COUP-TFI-O/E^{RV-Cre}*+LPS DG at 14dpi (one-way ANOVA F$_{(2;8)}$= 63.51, p<0.01, followed by Bonferroni post hoc test).

(**M**) Histograms reporting quantification of different YFP+ cell subtypes within the SGZ/GCL in *Ctrl^{RV-Cre}*+Saline, *Ctrl^{RV-Cre}*+LPS, and *COUP-TFI-O/E^{RV-Cre}*+LPS DG at 14dpi. GFAP+YFP+ astrocytes: one-way ANOVA F$_{(2;8)}$= 5.394, p=0.0329, with Bonferroni post hoc test: *Ctrl^{RV-Cre}*+Saline *vs Ctrl^{RV-Cre}*+LPS, p>0.05; *Ctrl^{RV-Cre}*+LPS *vs COUP-TFI-O/E^{RV-Cre}*+LPS, *p<0.05; *COUP-TFI-O/E^{RV-Cre}*+LPS *vs Ctrl^{RV-Cre}*+Saline, p>0.05; DCX+YFP+ neurons: one-way ANOVA F$_{(2;8)}$= 2.015, p=0.1956, with Bonferroni post hoc test: *Ctrl^{RV-Cre}*+Saline *vs Ctrl^{RV-Cre}*+LPS, p>0.05; *Ctrl^{RV-Cre}*+LPS *vs COUP-TFI-O/E^{RV-Cre}*+LPS, p>0.05; *COUP-TFI-O/E^{RV-Cre}*+LPS *vs Ctrl^{RV-Cre}*+Saline, p>0.05. GCL, granule cell layer.

N=3/4 animals per genotype. Error bars indicate SEM. Scale bars: H, 10µm. Student's t-test *p<0.05; ***p<0.001.

SUPPLEMENTAL TABLE

Table S1. Phenotypes of YFP+ cells expressed as percentages of marker(s)+YFP+ cells among all YFP+ cell population in the SGZ+GCL of the hippocampal DG in control and mutant mice. Related to Figures 3,4,5,6.

	Mean ± SEM (cell numbers)		Statistical values (Two-tailed unpaired Student's t-test)
	Ctrl^{Glast}	*COUP-TFI-icKO^{Glast}*	
% DCX+/ **YFP+ population**	Tam2w: 60.85 ± 6.84% (n=209/336 cells)	Tam2w: 26.91 ± 2.16% (n=86/316 cells)	P<0.01 (**)
% NeuroD+/ **YFP+ population**	Tam2w: 40.87 ± 2.55% (n=136/332 cells)	Tam2w: 28.45 ± 1.30% (n=93/325 cells)	P<0.05 (*)
% NeuN+/ **YFP+ population**	Tam7.5w: 62.29 ± 1.52% (n=314/502 cells)	Tam7.5w: 20.97 ± 1.88% (n=230/1090 cells)	P<0.001 (***)
% GFAP+ astrocytes/ **YFP+ population**	Tam2w: 16.64 ± 2.66 % (n=45/275 cells) Tam7.5w: 16.48 ± 1.26% (n=48/294 cells)	Tam2w: 26.69 ± 0.59% (n=66/251 cells) Tam7.5w: 29.11± 0.63% (n=166/569 cells)	Tam2w: P<0.05 (*) Tam7.5w: P<0.001 (***)
% s100b+ astrocytes/ **YFP+ population**	Tam2w: 8.71 ± 1.24 % (n=27/291 cells) Tam7.5w: 9.67 ± 1.13% (n=30/312 cells)	Tam2w: 18.32 ± 1.08% (n= 53/287 cells) Tam7.5w: 28.98± 2.02% (n=135/486 cells)	Tam2w: P<0.001 (***) Tam7.5w: P<0.01 (**)
% GFAP+ RGL cells/ **YFP+ population**	Tam2w:15.63 ± 3.42%, (n=42/275 cells)	Tam2w: 16.32 ± 3.11%, (n=39/251 cells)	P=0.8871 (ns)
	Ctrl^{Ascl1}	*COUP-TFI-icKO^{Ascl1}*	
% DCX+/ **YFP+ population**	84.50 ± 0.86% (n=222/263 cells)	48.13 ± 0.41% (n=160/332 cells)	P<0.001 (***)
% GFAP+Sox2+ **astrocytes/** **YFP+ population**	2.74 ± 0.47% (n=10/359 cells)	13.63 ± 2.39% (n=60/413 cells)	P<0.05 (*)
	Ctrl^{Glast}	*COUP-TFI-O/E^{Glast}*	
% DCX+/ **YFP+ population**	50.64 ± 1.70% (n=543/1068 cells)	55.91 ± 6.39% (n=75/1045 cells)	P=0.5096 (ns)
% GFAP+ astrocytes/ **YFP+ population**	20.41 ± 2.19% (n=214/1068 cells)	8.84 ± 1.20% (n=75/1045 cells)	P<0.001 (**)
% GFAP+ RGL cells/ **YFP+ population**	10.65 ± 0.93% (n=117/1068 cells)	13.85 ± 1.95% (n=118/1045 cells)	P=0.2135 (ns)

N=3-4/genotype/time-point. Values are expressed as mean ± SEM; ns=not significant.

SUPPLEMENTAL EXPERIMENTAL PROCEDURES

Animals and housing conditions

Mice were genotyped as previously published (Armentano et al., 2007; Mori et al., 2006; Srinivas et al., 2001; Battiste et al., 2007; Wu et al., 2010). All mouse lines were maintained in a C57BL/6J genetic background and were 8-12 weeks old at the onset of the experiments. Both male and female transgenic mice were included in the analysis of COUP-TFI deletion/overexpression. Mice were housed in standard cages (n=2-4 mice/standard cage) under a 12 h light/dark cycle with access to food and water *ad libitum*.

LPS, tamoxifen and BrdU administrations

To induce a cellular/molecular cascade able to initiate an inflammatory response, a systemic administration of the *E. coli*-derived lipopolysaccharide (LPS, SIGMA, L2880) was dissolved in sterile physiological solution and injected intraperitoneally into adult mice for either 1 or 4 consecutive days at the dose of 0,5 mg/kg/day.

For activation of the CreERT2 recombinase in Glast-lineage, animals were administered with tamoxifen (TAM, SIGMA, T-5648) at the dose of 2,5 mg/mouse/day dissolved into cornoil (SIGMA) by means of gavage for either 5 (for the short-term analysis) or 2 consecutive days (for the long-term analysis). For activation of the CreERT2 recombinase in Ascl1-lineage, P60 animals were administered with gavage for 5 consecutive days.

5-bromo-2-deoxyuridine (BrdU, SIGMA) was intraperitoneally injected (BrdU dose/inj.=100 mg/kg, calculated based on the weight of the animal) after TAM treatments in the Glast-dependent lineage. To assess proliferation, mice treated with TAM for 5 days received three BrdU injections 2 hours apart on day 2 after the last TAM treatment (i.e. 1 day before sacrifice). For analysis of cell survival, two BrdU injections, 8-hours apart, were performed on day 11 after the last TAM treatment on animals that received 2 days TAM administration; animals were euthanized 3 and 17 days post BrdU injection.

Retro-Cre retrovirus stereotaxic injection in the adult DG

Adult mice *R26-YFP+/+;COUP-TFIfl/fl (COUP-TFI-cKO^{RV-Cre}), R26-YFP+/+;COUP-TFIwt/wt (Ctrl^{RV-Cre}), R26-YFP+/+;hCOUP-TFI+/wt (COUP-TFI-O/E^{RV-Cre})* were anesthetized in a constant flow of Isofluorane (3%) in oxygen, positioned in a stereotaxic apparatus (Stoelting) and injected with a pneumatic pressure injection apparatus (Picospritzer II, General Valve Corporation). The skull was exposed by an incision in the scalp and a small hole (about 1 mm) drilled through the skull. 1 μl of retrovirus-Cre (RV-pMIG::Cre; titer 2.7x10^7, Rolando et al., 2016) was injected in the DG using a sharpened glass capillary at the following stereotaxic coordinates: -2 mm (antero-posterior), 1.5 mm (lateral) to Bregma and -2.0 mm below the surface of the skull. Mice (n=4/5 genotype/experiments) were killed 2, 14 or 18 days after virus infection. Brain tissue was processed and analyzed by immunohistochemistry as described above.

Tissue collection, RNA extraction and RT-qPCR

Adult mice were perfused with ice-cold PBS. Hippocampi were microdissected and lysed, and RNA isolation was performed using RNeasy Micro Kit (Qiagen, France). Reverse transcription was carried out using QuantiTect kit (Qiagen, France). The qPCR reactions were performed in duplicates in a LightCycler480 (Roche) using QuantiTect SYBR Green PCR kit (Qiagen, France) and gene-specific primers (see Table). The amount of transcripts was evaluated relatively to the expression level of the housekeeping gene acidic ribosomal phosphoprotein P0 (Rplp0 or 36B4). Fold change was calculated with respect to control saline-injected group.

Tissue preparation

For immunostaining experiments, adult mice were deeply anesthetized with an intraperitoneal injection of a mixture of ketamine (75 mg/kg; Ketavet; Gellini) and xylazine (30 mg/kg; Rompun; Bayer) and perfused transcardially with ice-cold 0.9% saline solution, followed by ice-cold 4% paraformaldehyde (PFA) in 0.1 M phosphate buffer (PB), pH 7.4. Brains were removed from the skull, postfixed for 4 hours in the same PFA solution, cryoprotected in a 30% sucrose solution (in 0.1 M PB, pH 7.4), OCT-embedded, frozen at -80°C and finally sectioned using cryostat (Leica Microsystems). Free floating coronal serial sections (30μm for Glast- and Ascl1-lineage experiments, 40μm for retroviruses experiments) were collected in multi-well dishes. Sections were stored at −20°C in antifreeze solution until

use. For *in situ* hybridization, after dissection, brains were postfixed overnight in 4% PFA and specimens were then processed as described above except of cryostat coronal sections (16 μm), which were collected in series directly on Superfrost Plus glass slides (Thermo Scientific).

Immunofluorescence and immunohistochemistry

Immunofluorescence (IFL) reactions for BrdU and selected markers were performed on free floating coronal serial sections as detailed below: sections were incubated either overnight (o/n) or for 48 hours at 4°C with primary antibodies (**Table**) diluted in 0.01M PBS (pH 7.4), 0.5% Triton X-100, and 1% normal serum of the same species of the secondary antibody (normal donkey serum, NDS). Sections were washed in PBS and incubated for 1 hour at room temperature with secondary antibodies (**Table**) in 0.01 M PBS (pH 7.4), 0.5% Triton X-100, and NDS (1%). Sections were washed in 0.01M PBS (pH 7.4) and incubated for 15 minutes at room temperature with 4,6-diamidino-2-phenylindole (DAPI, 1 μg/ml) to label nuclei. Sections were washed in 0.01M PBS (pH 7.4) then mounted on gelatine coated slides, air dried, and coverslipped with antifade mounting medium Mowiol (4-88 reagent, Calbiochem 475904). For double and triple immunostaining with BrdU and other antigens: first, sections were incubated with the antibody/antibodies for the other antigens followed by secondary antibody/antibodies in the same way mentioned above. These sections were pre-treated with 2N HCl for 35 min at 37°C to denature DNA and neutralized with borate buffer (pH 8.5) for 10 min. Sections were then incubated with anti-BrdU and secondary antibody followed by DAPI staining, mounted and coverslipped as above. For immunostaining with mouse anti-Nestin and anti-Ascl1 a five minute-long antigen retrieval treatment with pre-heated citrate buffer (0.1M, pH6) was performed. For the avidin-biotin-peroxidase method, sections were incubated for 1 h at room temperature in secondary biotinylated antibody diluted 1:250 in 0.01 M PBS, pH 7.4, followed by the avidin-biotin-peroxidase complex (Vector Lab). To reveal immunoreactivity, we used 0.015% 3,3'-diaminobenzidine (DAB) and 0.0024% H_2O_2 in 0.05M Tris-HCl, pH 7.6. After adhesion on gelatin coated glass slides, sections were dehydrated and mounted in Sintex (Nuova Chimica).

In situ hybridization

Briefly, for the preparation of the antisense riboprobe for COUP-TFI a plasmid containing COUP-TFI encoding sequence was linearized by using a specific restriction enzyme (EcoRI; BioLabs Inc.), filtered and the transcription of the antisense RNA probe was performed by using a specific RNA Polymerase (T3; Promega) according to the manufacturer's instructions. After a treatment with DNAse (RNAse-free; Roche) the probe was precipitated o/n at -20°C in a solution containing LiCl 0.1M and EtOH followed by a series centrifugation at 4°C. The RNA probe pellet was finally suspended in sterile H_2O. *In situ* hybridization for COUP-TFI on cryostat-cut adult brain sections were performed as follows. Defrosted and dried adult brain sections were treated with RIPA buffer (150 mM NaCl, 1% NP-40, 0.5% Na deoxycholate, 0.1% SDS, 1 mM EDTA, 50 mM Tris, pH 8.0) twice for 10 min and then postfixed 15 min in 4% PFA. Pre-hybridization (1.5h) and hybridization (o/n) of the sections with digoxigenin (DIG)-labelled riboprobes were performed at 70°C in the following solution: 50% formamide, 5 SSC, 5 Denhardts solution (Invitrogen), 500 mg ml 1 Salmon Sperm DNA (Ambion) 250 mg ml 1 Yeast t-RNA. The day after, slides were washed twice for 1 h at 70°C in the following solution: 50% formamide, 2 SSC, 0.1% Tween 20. Then, the samples were equilibrated in MABT solution and blocked in MABT/10% sheep serum to detect the hybridized riboprobes by the use of an anti-DIG antibody (1:2000, Roche) overnight at 4°C. Finally, sections were washed several times in MABT, equilibrated in B3 buffer (100 mM Tris, pH 9.5, 50 mM MgCl2, 100 mM NaCl, 0.1% Tween-20) and the antibody was detected by incubating the slices in NBT/BCIP solution (Roche) at room temperature. The riboprobe for COUP-TFI were synthesized by the use of DIG RNA labelling kit (Roche) following manufacturer's instructions.

Microscope analysis and cellular quantification

Representative images showing ISH and IHC for COUP-TFI were photographed on a Nikon microscope coupled with a computer-assisted image analysis system (Neurolucida software, MicroBrightField). Images of multiple labelled sections by means of immunofluorescence were acquired with a TCS SP5 confocal microscope (Leica). Confocal image z-stacks were captured through the thickness of the slice (30/40 μm) at 1-μm optical steps with an objective 40X/1.25-0.75 (oil immersion lens), zoom (1.2) and resolution of 1024/1024 pixels and 100Hz comprising both upper and lower blades of the DG. Images were then analysed with NIH ImageJ (http://rsb.info.nih.gov/ij) using the cell counter and channel tools plug-ins.

For the characterization of COUP-TFI expression within the DG, cells labelled with different markers (BLBP, GFAP/Nestin, Ascl1, Ki67, NeuroD1, DCX, NeuN, Sox2, S100B) were analyzed for the co-expression of COUP-TFI on images captured at the confocal microscope. At least three different levels among the rostro-caudal extention of the DG (bregma: from -1.30 to -3.80) were analysed and around 100-200 marker-positive cells were counted per animals

(n=3 mice per counting). For COUP-TFI ablation and overexpression experiments (Glast-/Ascl1-lineages), marker+YFP+ cells were quantified in confocal images (50-150 YFP+ cells/slice; n=3-5 animals/genotype). DAPI staining was used to trace the granule cell layer in DG of the hippocampus and to counterstain clustered cells and be able to discriminate single YFP+ cells among packaged YFP+ cells. At least three rostro-caudal levels per animal were analysed, taking into account both upper and lower blades of the DG (as above). For analysis of GFAP+YFP+ RGL, cells were deemed to be radial if the cell body, clearly associated with a DAPI+ nucleus, was located in the SGZ and had a single thin radial process extending throughout GCL and branching into the MCL. The cell density (D) was calculated by dividing the total number of counted cells over the area of interest (SGZ, SGZ+GCL, or MCL) and expressed as mean number of cells per squared millimetres (cells/mm2; n=3-5 animals/genotype).

To compare COUP-TFI immunoreactivity levels in the nuclei of BLBP+ RGLs to the ones present in NeuroD+ neuronal progenitors within the same tissue samples, we manually drew an outline around the nucleus of each marker+ cell and we measured the mean fluorescence intensity of COUP-TFI staining within each nuclei, a value that is independent from the nucleus size. Finally, we normalized the mean intensity of staining of each COUP-TFI+ nuclei by subtracting to each obtained value the background (i.e., a region within the same frame that has no COUP-TFI staining). For each animal, a mean value was calculated from all the sections counted, and for each genotype, a mean value was obtained by pooling the means of the sampled animals.

Gene-specific primers for RT-qPCR

Gene	Forward	Reverse
IL1A	TGCAGTCCATAACCCATGATC	ACAAACTTCTGCCTGACGAG
IL1β	ACGGACCCCAAAAGATGAAG	TTCTCCACAGCCACAATGAG
TNFα	CTTCTGTCTACTGAACTTCGGG	CAGGCTTGTCACTCGAATTTTG
DCX	CAGTCAGCTCTCAACACCTAAG	CATCTTTCACATGGAATCGCC
NeuroD	CTCCAGGGTTATGAGATCGTC	GTCCTGAGAACTGAGACACTC
COUP-TFI (NR2F1)	AACTGGCCTTACATGTCCATC	ATCATACCAGCATCCCCAAAG
GFAP	GAAAACCGCATCACCATTCC	CTTAATGACCTCACCATCCCG
Rplp0 (36B4)	ACCCTGAAGTGCTCGACATC	AGGAAGGCCTTGACCTTTTC

List of primary and secondary antibodies

Antigen name	Host	Dilution	Source	Catalogue number
Primary antibodies				
Ascl1 (Mash1)	Mouse	1:500	BD Pharmingen	556604
BLBP	Rabbit	1:1000	Abcam	ab32423
BrdU	Rat	1:3000	AbD Serotec	OBT0030CX
Cleaved Caspase-3	Rabbit	1:300	Cell Signalling	9961
COUP-TFI	Mouse	1:500	R&D System	PP-H8132-10
COUP-TFI	Rabbit	1:700	M. Studer's lab	-
DCX	Goat	1:1500	Santa Cruz Biotechnology	Sc-8066
GFAP	Rabbit	1:2000	Dako	Z 0334
GFAP	Goat	1:200	Abcam	ab53554
GFP	Chicken	1:1000	AvesLab	GFP-1020
Ki67	Rabbit	1:1000	Novocastra (Leica)	NCL-Ki67p
MCM2	Goat	1:500	Santa Cruz Biotechnology	Sc-9839
Nestin	Mouse	1:500	Millipore	MAB353
NeuN	Mouse	1:1000	Chemicon	MAB377
NFIA	Rabbit	1:1200	Abcam	41581
NeuroD1 (NeuroD)	Goat	1:400	Santa Cruz Biotechnology	Sc-1804
S100B	Rabbit	1:10000	Swant	37A
Sox2	Rabbit	1:1000	Chemicon	AB5603
Sox2	Goat	1:200	Santa Cruz Biotechnology	Y-17
Sox10	Goat	1:1000	Santa Cruz Biotechnology	Sc-17342
Secondary antibodies				
AlexaFluor488 Anti-Ck	Donkey	1:400	Jackson ImmunoResearch	703-545-155
AlexaFluor488 Anti-Gt	Donkey	1:400	Jackson ImmunoResearch	705-545-147
AlexaFluor488 Anti-Ms	Donkey	1:400	Jackson ImmunoResearch	715-545-151
AlexaFluor488 Anti-Rb	Donkey	1:400	Jackson ImmunoResearch	711-545-152
AlexaFluor488 Anti-Rt	Donkey	1:400	Jackson ImmunoResearch	712-545-153
AlexaFluor647 Anti-Gt	Donkey	1:600	Jackson ImmunoResearch	705-605-147
AlexaFluor647 Anti-Ms	Donkey	1:600	Jackson ImmunoResearch	715-605-151
AlexaFluor647 Anti-Rb	Donkey	1:600	Jackson ImmunoResearch	711-605-152
AlexaFluor647 Anti-Rt	Donkey	1:600	Jackson ImmunoResearch	712-605-153
Cy3 Anti-Ms	Donkey	1:800	Jackson ImmunoResearch	715-165-151
Cy3 Anti-Gt	Donkey	1:800	Jackson ImmunoResearch	705-165-147
Cy3 Anti-Rb	Donkey	1:800	Jackson ImmunoResearch	711-165-152
Cy3 Anti-Rt	Donkey	1:800	Jackson ImmunoResearch	712-165-153
Biotinylated anti-Rb	Horse	1:250	Vector Labs	BA-1100